Aus dem Institut für Veterinär-Physiologie
des Fachbereiches Veterinärmedizin
der Freien Universität Berlin

Identification of Metabolic Prognostic Markers in Liver Diseases After Carbon Tetrachloride Intoxication

Inaugural-Dissertation
zur Erlangung des Grades eines
Doktors der Veterinärmedizin
an der
Freien Universität Berlin

vorgelegt von
Amnah Hofney Othman
Tierärztin
aus El Minia (Ägypten)

Berlin 2018
Journal-Nr.: 4053

mbvberlin | mensch und buch verlag

Aus dem Institut für Veterinär-Physiologie
des Fachbereiches Veterinärmedizin
der Freien Universität Berlin

Identification of Metabolic Prognostic Markers in Liver Diseases After Carbon Tetrachloride Intoxication

Inaugural-Dissertation
zur Erlangung des Grades eines
Doktors der Veterinärmedizin
an der
Freien Universität Berlin

vorgelegt von
Amnah Hofney Othman
Tierärztin
aus El Minia (Ägypten)

Berlin 2018
Journal-Nr.: 4053

Gedruckt mit Genehmigung des Fachbereichs Veterinärmedizin
der Freien Universität Berlin

Dekan:	Univ.-Prof. Dr. Jürgen Zentek
Erster Gutachter:	Univ.-Prof. Dr. rer. nat. Salah Amasheh
Zweiter Gutachter:	Univ.-Prof. Dr. rer. nat. Steven Dooley
Dritter Gutachter:	Univ.-Prof. Dr. Wolfgang Bäumer

Deskriptoren (nach CAB-Thesaurus):
mice, animal models, fibrosis, liver diseases, liver functions, diagnostic techniques, nuclear magnetic resonance spectroscopy, carbon tetrachloride

Tag der Promotion: 17.05.2018

Bibliografische Information der *Deutschen Nationalbibliothek*
Die Deutsche Nationalbibliothek verzeichnet diese Publikation in der Deutschen Nationalbibliografie; detaillierte bibliografische Daten sind im Internet über <https://dnb.de> abrufbar.

ISBN: 978-3-86387-912-9
Zugl.: Berlin, Freie Univ., Diss., 2018
Dissertation, Freie Universität Berlin
D188

 Choriner Str. 85 - 10119 Berlin
verlag@menschundbuch.de – www.menschundbuch.de

TABLE OF CONTENTS

TABLE OF CONTENTS

LIST OF ABBREVIATIONS

NMR:	Nuclear Magnetic Resonance
HCC:	Hepatocellular Carcinoma
HSC:	Hepatic stellate cell
CCl_4:	Carbon Tetrachloride
^{1}H-MAS-NMR:	Proton-Magic Angle Spinning NMR
MS:	Mass spectroscopy
IR:	Infrared spectroscopy
FID:	Free Induction decay
DSS:	Sodium 3-(trimethylsilyl)-1-propanesulfonate
CPMG:	Carr, Purcell, Meiboom -Gill spin-
PBS:	Phosphate Buffer Saline
H&E:	Hematoxylin and Eosin
BSA:	Bovine serum albumin
α-SMA:	Alpha smooth muscle actin
PSR:	Picrosirius red
IHC:	Immunehistochemistry
CYP2E1:	Cytochrome P450 2E1
GS:	Glutamine synthetase
TSP:	Sodium 3-trimethylsilyl-1-propanesulfonate
D_2O:	Deuterium Oxide
ALT:	Alanine aminotransaminase
AST:	Aspartate aminotransaminase
ROC:	Receiver operating characteristic curve
AUC:	Area Under the Curve
LY2157299:	Galunisertib
PSMAD2:	Phosphorylated Smad2
ALK5:	TGFβ type I receptor kinase

LIST OF FIGURES

LIST OF TABLES

INTRODUCTION

Currently, the diagnosis of liver diseases is based on histological assessments of biopsies. The use of liver biopsies, however, is not without cost or risk (bleeding, perforation, death). Furthermore, while regarded as a gold standard for diagnosis, a liver biopsy can be subject to sampling and inter- and intra-observer variability. These limitations carry significant implications for clinical trials as the diagnostic accuracy, reliability, and responsiveness of treatment end-points impact trial size requirements, feasibility and costs. Furthermore, translating these findings to routine practice is difficult given the inability to perform routine frequent liver biopsies clinically. Thus, an urgent medical need exists for reliable and highly accurate surrogate end-points that can be used instead of liver biopsies. This will be of substantial importance in early-phase clinical trials, and will help to ensure clinical trial findings are readily translatable and measurable in routine practice.

The liver is a major metabolic organ. Acute, chronic, acute-on-chronic and cancer conditions perturb the regulation of metabolism at different levels. From this point of view, the blood or urine metabolome should represent the final outcome of liver metabolic regulation, and for this reason represent the phenotype of a specific disease and the disease stage (Amathieu et al., 2016).

Nuclear magnetic resonance (NMR) is a promising tool for metabolic profiling. During acute liver injury, urine metabolomics has been performed using NMR to study the secondary metabolism of acetaminophen (Clayton et al., 2009). Moreover, Winnike et al. (2010) used a pharmaco-metabolomics approach to predict acetaminophen-induced liver injury with a therapeutic dose in urine. Therefore, an NMR-based metabolomics approach could be a practical method for identifying susceptible patients shortly after starting drug treatment and with a high risk of developing drug induced liver injury. In acute liver failure, it has been shown that glutamine could allow to predict an unfavorable outcome with a high sensitivity (Saxena et al., 2006). Several studies have described a close relationship between metabolic abnormalities and the severity of alcohol-induced cirrhosis in sera and tissues

(Amathieu et al., 2011; Martínez-Granados et al., 2006). Another study shows that metabolomics can identify the differences between compensated and decompensated cirrhosis, caused by alcohol consumption (Qi et al., 2012). In the aforementioned reports, several metabolites were identified and they reflected major changes in liver function such as energy-, urea- or amino-acid metabolism.

Aims of the study

The fundamental challenge to be addressed is to establish and validate diagnostic marker(s) for liver diseases based on metabolite levels. Therefore, the scope of this proposed study will encompass the following aspects: 1) Metabolite screening for diagnosis and staging, and more specifically, to identification of the presence and the severity of inflammation and fibrosis in murine livers and blood, 2) Searching for biomarkers that can predict liver disease progression, and 3) Matching our findings with publically available microarray datasets (genomics) in patient cohorts and experimental data (mouse experiments). The ultimate goal of the present study is to identify metabolite(s), the levels of which are affected by liver disease progression.

REVIEW OF LITERATURE

2.1. Liver Physiology and Histology

The liver is a complex metabolic organ. It has pivotal roles in metabolism homeostasis as e.g. synthesis and storage of carbohydrates, lipids and proteins. Moreover, the liver plays a central role for detoxification mechanisms (Boyer et al., 2006; Braeuning et al., 2010; Godoy et al., 2013). The liver is converting ammonia to urea and controlling the glucose level by glycolysis, gluconeogenesis and glycogenolysis, which are considered important steps for ammonia detoxification and glucose homeostasis, respectively, in whole organisms (Moorman et al., 1989; Ghafoory et al., 2013; Hijmans et al., 2014). These different metabolic capacities are mainly hosted by hepatocytes (Michalopoulos and Khan 2005; Michalopoulos, 2007; Godoy et al., 2013). Beside aforementioned functions, the liver is considered a glandular organ because it secretes bile. In addition, the liver plays an essential role in the storage of vitamins and iron, in breaking down hemoglobin and insulin as well as in the production of different coagulation factors and immunoglobulins (Bacon et al., 2006).

The liver is located in the upper right part of the abdominal cavity and is connected to the diaphragm. This unique anatomical position of the liver facilitates both metabolic and biochemical transformation functions (Barberá-Guillem et al., 1990; Sahu, 2007). Therefore, the liver receives blood containing substances absorbed or secreted by the gastrointestinal tract, spleen and pancreas. Then, these substances are returned to the blood stream or to the bile for elimination. The mouse liver consists of four main lobes caudate lobe, right lobe, median lobe and left lobe (Hollander et al., 1987; Martins et al., 2008). Histologically, the hepatic lobule is considered a classical unit of the organ. It is a polygon with portal triads at the corners. It consists of radially arranged plates of approximately 25 hepatocytes from the portal compartment to the central vein (Rappaport, 1973; Krishna, 2013). The portal triad contains microscopic branches of bile duct, hepatic artery and portal vein. Metabolically, the functional unit is called hepatic acinus (Gumucio and Miller, 1982; Bacon et al., 2006). The axis of the hepatic acinus is a portal tract and its boundary is

described by an imaginary line connecting the neighboring terminal central veins. The hepatic acinus is divided into three zones of hepatocytes. Each zone has different levels of nutrients and oxygen supply as well as a different metabolic function (Bacon et al., 2006). Zone I (periportal compartment) is supplied with blood rich in oxygen, hormones and substrates. However, zone II (mid-zonal compartment) and zone III (perivenous compartment) are supplied by blood poor in oxygen but rich in carbon dioxide and metabolic products (Gebhardt, 1992; Katz, 1992; Hijmans et al., 2014). This remarkable hepatocyte heterogeneity along the porto-central axis with respect to levels of oxygenation and nutrition is resulting in different cellular functions, e.g. gluconeogenesis and oxidative phosphorylation are performed by periportal hepatocytes. However, xenobiotic metabolism, glycolysis, and lipogenesis occur mainly in the perivenous compartment (Gebhardt, 1992; Ghafoory et al., 2013). In addition to liver parenchymal cells (hepatocytes), the liver consists of liver endothelial sinusoidal cells (LESC), hepatic stellate cells (HSCs), Kupffer cells and cholangiocytes (biliary epithelial cells) (Boyer et al., 2006; Böhm et al., 2010).

2.2. Metabolic profiling of the liver starts with physiology

Metabolic profiling and finger printing is considered a key process in the pharmaceutical industry to study drug efficiency or toxicology (Gebhardt, 1992). In clinical research, metabolic profiling helps to identify biomarker compounds for early disease detection, monitoring and allows studying the effects of drugs in biological systems in a rapid and robust way. Liver diseases are characterized by a high mortality rate and complicated pathogenesis as well as by significant individual differences. Until now, there is only an invasive method that available to diagnose the stages of the diseases. Recently, a number of investigations focused on molecular biology, proteomics and metabolomics. Metabolomics is an investigation of biological systems where changes in metabolites after specific stimulation or even treatment with toxic substances are determined. This type of investigation mainly focuses on the end products of the biological systems, which are

reflection of both the physiological and biochemical status. The introduction of metabolomics can provide us with much information about liver diseases. The current strategy of the metabolomics investigation on liver diseases is to measure and to identify metabolites in blood plasma and urine. Tissue metabolic profiling has indeed several advantages: The correlation between metabolite levels in tissue and body fluids reflects the pathogenesis alteration in certain tissue. Several reports have estimated the levels of metabolites involved in hepatocellular carcinoma (HCC) e.g. beta-sitosterol, L-phenyl alanine, lyso-PCs and glycerophosphocholine (Baniasadi et al., 2013). The aforementioned metabolites were significantly higher in HCC tissues compared to healthy livers (Nwosu et al., 2017). Glutamate plays a pivotal role in the metabolism of the hepatic amino acids e.g. in the transdeamination of most amino acids, the catabolism of arginine, ornithine, oroline, and the conversion to glutamine (Amathieu et al., 2011; Martínez-Granados et al., 2006). It is now well known that different hepatic function is always associated with hepatocyte subpopulations with different acinar zones.

2.3. Hepatocyte

The liver cell (hepatocyte) is a big polyhedral cell. It is about 20-30 μm in size and has a volume of approximately 5000 μm^3 (Boyer et al., 2006). Hepatocytes represent 80% of the liver volume and more than 65% of the total liver cells (Godoy et al., 2013). It is a typical epithelial cell and polarized with well characterized apical, lateral and basal membranes. The basal membranes of hepatocytes face the sinusoidal endothelium (so called sinusoidal membrane). However, the apical surfaces form between two adjacent hepatocytes and enclose the bile canaliculi (therefore, it is called canalicular surface). Moreover, the lateral membranes of hepatocytes extend from the bile canaliculi to the Disse space and form cell–cell junctions, including gaps (to facilitate communication between hepatocytes) and tight junctions (to seal the bile canalicular lumen from the interstitial space). Hepatocytes have one nucleus although nearly 40% are binucleated (Boyer et al., 2006). The cytoplasm of the hepatocyte contains numerous mitochondria, a prominent Golgi apparatus located between the nucleus and the bile canaliculi, rough and smooth endoplasmic reticulum. Liver cells

also contain numerous endosomes, lysosomes and peroxisomes. The lifespan of hepatocytes is approximately 400 days (Magami et al., 2002; Wang et al., 2011) in mice. Hepatocytes play significant roles in various aspects of liver physiology and pathology.

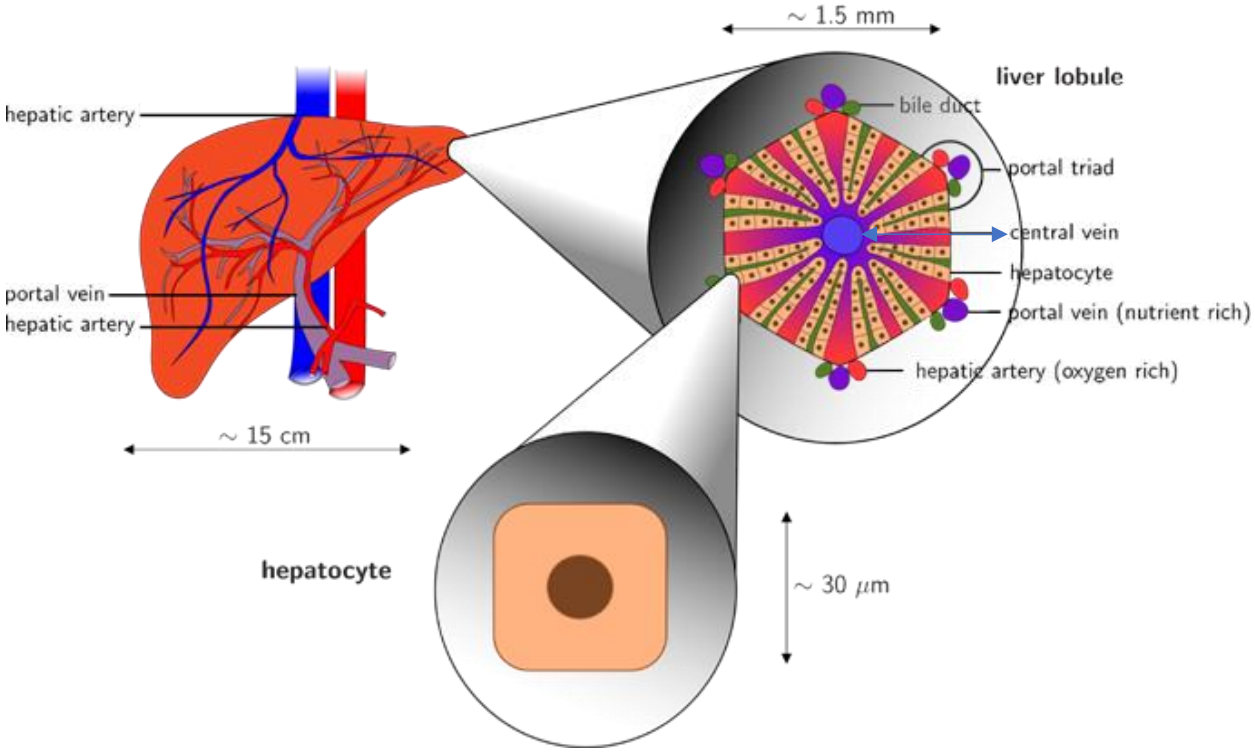

Figure 2.3: Lobular and cellular liver structure (Source: modified from Ricken et al., 2015).

2.4. Hepatic stellate cell (HSC)

Hepatic stellate cells (known as Ito cells, perisinusoidal cells or lipocytes)- are fat storing cells in normal liver (quiescent state). HSCs lie in the Disse space between the hepatocyte and liver sinusoidal endothelial cells. Quiescent HSCs represent 5-8% of the total number of liver cells (Geerts, 2001; Stanciu et al., 2002; Godoy et al., 2013). However, during liver damage, HSCs start to change their phenotype into an activated state. Activated HSCs are characterized by proliferation, contractility, migration and chemotaxis as well as, most importantly, by extracellular matrix production. The role of the activated HSC during the

liver damage is well known and described in several reports (Bataller and Brenner, 2005; Friedman, 2008; Krizhanovsky et al., 2008).

2.5. Model of hepatic damage and regeneration response

The liver has a unique capacity to detoxify various xenobiotics. This detoxification process evolved to protect animals from plant and food toxins (Michalopoulos, 2007). In addition to the detoxification potential, the liver is able to regenerate after exposure to different insults as e.g. to hepatotoxins. The regenerative potential of the liver has been fully described in Hesiod's Theogony (750 to 700 BC). Today, in several models a single toxic dose of carbon tetrachloride (CCl_4) produces massive centrilobular hepatocyte necrosis (Höhme et al., 2007; Hoehme et al., 2010; Zellmer et al., 2010; Hammad et al., 2014). Within 7 days, the necrotic area is morphologically regenerated (Hoehme et al., 2010). However, deposition of the extracellular matrix, so-called fibrosis, is observed only following multiple doses of CCl_4 (Krizhanovsky et al., 2008; Nussler et al., 2014). The pattern of liver fibrosis induced by CCl_4 is centrilobular (Hammad et al., 2017).

2.6. Toxicological implications of carbon tetrachloride (CCl_4)

The classical liver toxicity of carbon tetrachloride (CCl_4) is a complex process involving toxicological and necro-inflammatory processes. The centrilobular hepatic damage results from the cytochrome P-450 2E1-mediated bio-activation of CCl_4 in centrilobular hepatocytes (Shi et al., 1998; Manibusan et al., 2007) which have the highest concentration of cytochrome P450 2E1 (Raucy et al., 1993; Diaz Gomez et al., 2006). However, the CCl_4 mechanism of action is not yet fully understood. It is well known that the bio-activation of CCl_4 produces highly reactive free radical metabolites, especially, trichloromethyl / or trichloromethyl peroxyl free radicals (Poyer et al., 1980; Slater et al., 1985). Polyunsaturated fatty acids are attacked in the cell membranes by these free radicals which results in disruptions of cellular functions as well as of membrane integrity (Slater and Sawyer 1970). This mechanism is defined as lipid peroxidation. Lipid peroxidation causes

cellular stress and finally death of centrilobular hepatocytes (Weber et al., 2003; Hammad et al., 2017).

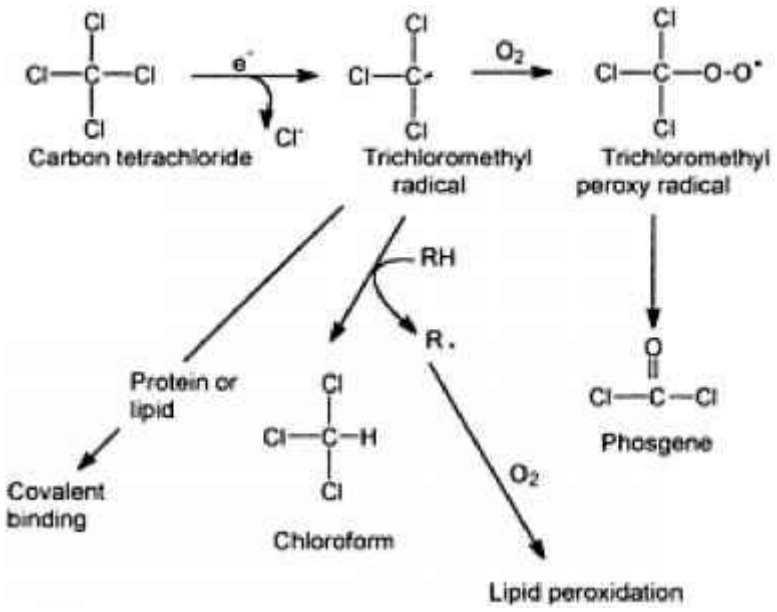

Figure 2.6: Biochemical reaction of carbon tetrachloride inside the cell (Source: http://www.europeanmedical.info/metabolic-activation/carbon-tetrachloride.html).

2.7. Metabolomics study

Metabolomics is considered one branch of the OMICs science and refers to the study of low molecular weight compounds within cells, tissue, biofluids or organisms. As metabolomics can be performed on body fluids, i.e. by its non-invasive or at least minimal invasive nature, it is considered an ideal tool for the pharmaceutical and clinical diagnosis of diseases and for biomarker discovery (Gao et al., 2015). Studying the metabolome in liver diseases and especially in liver fibrosis will help us to track the trend of the disease progression. Metabolomics studies in liver fibrosis by using ^{1}H-MAS-NMR is highly recommended as it helps to distinguish between fibrotic and non-fibrotic patients. There are frequent failures to diagnose liver diseases owing to lacking efficient non-invasive diagnostic methods (Embade et al., 2016).

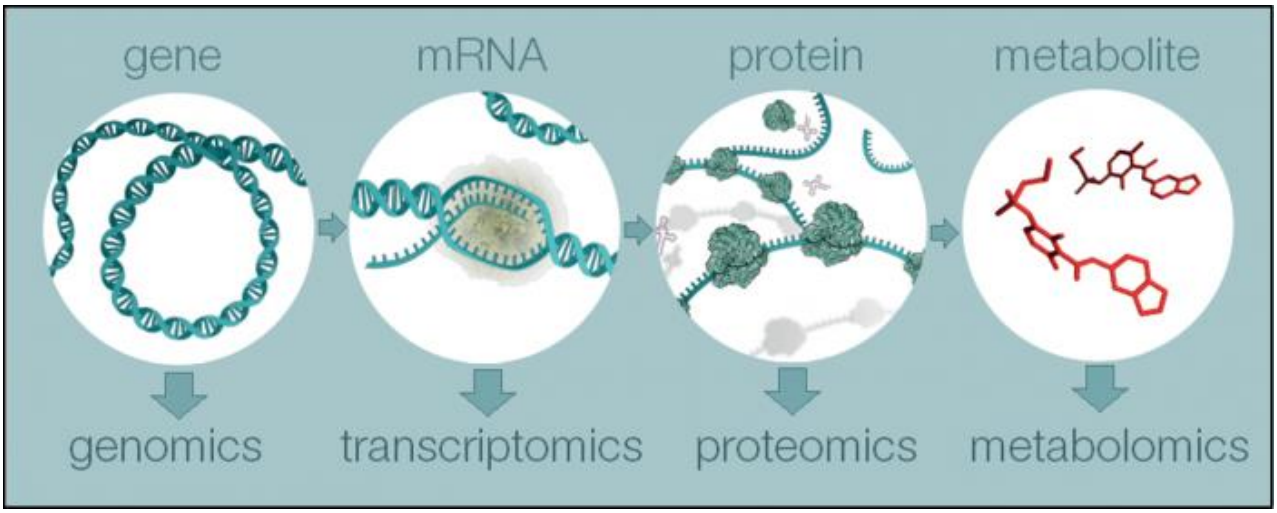

Figure 2.7: An overview of the four major "omics" fields, from genomics to metabolomics (Source: www.ebi.ac.uk/training/online/course/introduction-metabolomics)

2.8. Introduction to NMR spectroscopy

2.8.1. Applications of Nuclear Magnetic Resonance

NMR can be applied to numerous fields of research as e.g. structural (chemical) elucidation, in natural product chemistry or in synthetic organic chemistry. Moreover, it is frequently used as an analytical tool for synthetic chemists- used in conjunction with MS (mass spectrometry) and IR (infrared spectroscopy). Besides structural studies, NMR can deliver information on dynamic processes and chemical reaction kinetics. In biomedical applications, NMR is applied to structural (three-dimensional) studies of proteins, protein-ligand complexes, DNA, RNA as well as protein/DNA complexes. For the investigations in this thesis, NMR is applied to metabolomics, i.e. the identification and quantification of metabolites.

Figure 2.8.1: Nuclear magnetic resonance (NMR) magnet (600 MHz), (Source: https://phys.org/wire-news/145712162/animal-human-health-benefits-anticipated-from-universitys-premie.html).

2.8.2. Signals of Nuclear Magnetic Resonance

The NMR effect is shown by nuclei which have a nuclear spin, associated with a nuclear magnetic moment. While a classical magnetic moment can take any orientation in an external magnetic field, the atomic magnetic moments follow the rules of quantum mechanics. This means that just certain orientations with respect to the external field are possible. In case of the magnetic moment of the hydrogen (^{1}H) nucleus there is an orientation parallel and an orientation antiparallel to the external magnetic field B_0. Both these orientations show a difference in energy, with the higher energy level associated with the antiparallel orientation. For an ensemble of magnetic moments, the distribution between the two energy states is governed by the Boltzmann distribution, which says that there are more moments in the lower energy level than in the higher one. ^{1}H nuclei in a magnetic

field of 14.1 T have a difference in energy of $4.0 \cdot 10^{-25}$ J, which corresponds to a population difference of 1 in about 10.000 moments, following the Boltzmann distribution. NMR spectroscopy is, like other spectroscopies, based on the absorption and emission of electromagnetic radiation due to an energy difference. For a hydrogen nucleus in a magnetic field of B_0 = 14.1 T the frequency of the electromagnetic radiation is 600 MHz, which is called the resonance frequency. The algebraic sum of all individual magnetic moments in the sample adds up to a net magnetization vector, which shows in the direction of the B_0 field. When a strong electromagnetic pulse with a carrier frequency identical to the frequency difference is applied to the sample, the net magnetization vector is rotated from the B_0 direction to an axis perpendicular to the B_0 direction. This transverse magnetization is then detected with the receiver coil. The magnetization is, however, not stable and decays exponentially with a time constant T_2 denoted "spin spin relaxation time". For this reason, the signal delivered by the receiver coil sampled as a function of time shows the characteristic exponential decay pattern of a "free induction decay" (FID), see Figure 2.8.2. After calculating a Fourier transform of the time domain data the NMR spectrum is obtained. Another relaxation mechanism termed "spin lattice relaxation" describes the return of the magnetization distribution back to the thermodynamic equilibrium. The corresponding time constant is T_1 and is denoted "spin lattice relaxation time".

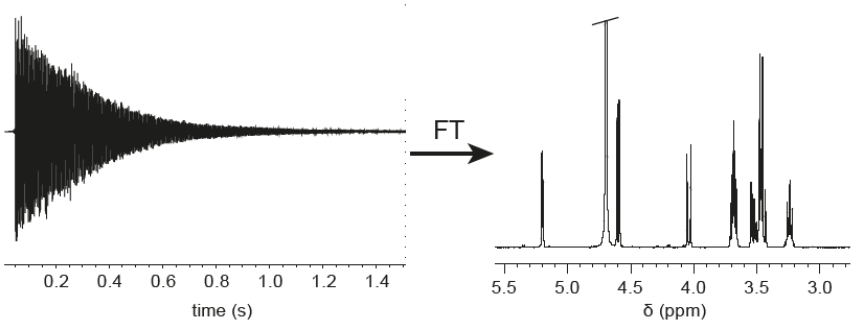

Figure 2.8.2: Signals in the time domain (FID) and in the frequency domain of NMR experiments.
(Source:https://chem.libretexts.org/Core/Analytical_Chemistry/Analytical_Sciences_Digital_Library/Active_Learning/In_Class_Activities/Nuclear_Magnetic_Resonance_Spectroscopy/03_Text/06_Classical_Description_of_NMR_Spectroscopy).

2.8.3 .The chemical shift

The nucleus is, however, not bare, but is surrounded by a cloud of electrons, which induce a local magnetic field at the site of the nucleus. The actual field at the site of the nucleus is thus determined by the density of the electrons surrounding the nucleus, i.e. nuclei with different environments have small differences in their resonance frequencies. In order to express the differences in resonance frequencies, the "ppm" scale is used, which is defined as the frequency difference of an arbitrary nucleus and a reference, divided by the frequency of the reference. In ^{1}H NMR spectroscopy, in aqueous solutions, sodium 3-(trimethylsilyl)-1-propanesulfonate (DSS) is a suitable reference, which corresponds to a ppm value of 0.

2.8.4. Peak area and proton counting

The area under a particular signal is always correlated to the number of protons giving rise to the NMR signal. The software of NMR spectrometers shows the signal integrals as a step curve plotted above the spectrum (see Figure 2.8.3).

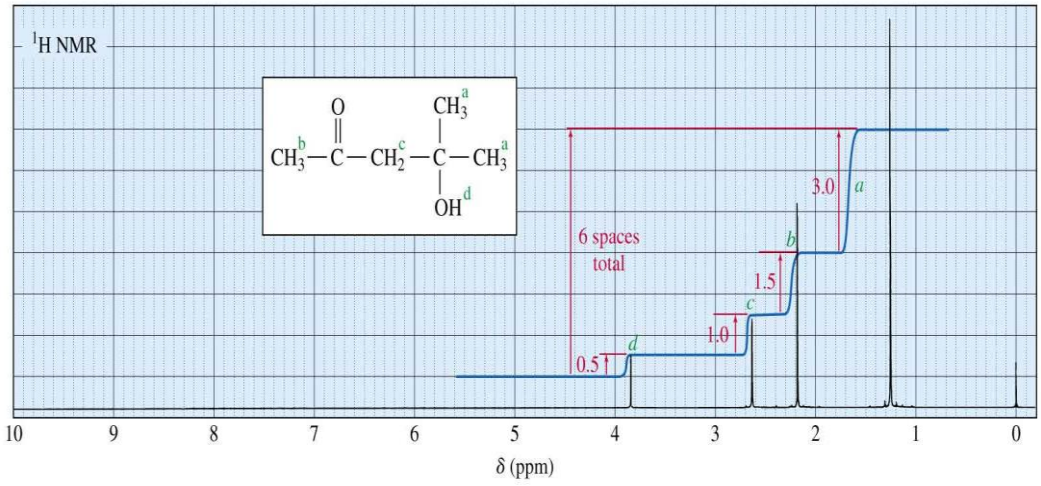

Figure 2.8.3: Peak area and proton counting in NMR (Source: https://www.slideshare.net/krishslide/nmr-spectroscopy-39462527).

2.8.5. High Resolution Magic Angle Spinning (MAS)-NMR spectroscopy for metabolic profiling of intact tissues.

The observation of metabolites within intact tissue by ^{1}H NMR spectroscopy is hampered by the broadening of the resonances due to effects like dipolar coupling, chemical shift anisotropy, and differences of bulk magnetic susceptibility. If the sample is spun at the magic angle $\theta = 54.7°$ (Figure 2), where θ is the angle between the sample tube and the B_0 field, many of these line broadening factors can be substantially reduced. This is due to the $(3 \cos 2 \theta - 1)$ angular dependence of two of the above mentioned interactions. For the line narrowing to be successful, a spinning rate comparable to the NMR line width of the tissue under static measurement settings has to be chosen. In order to avoid problems with spinning sidebands, at 600 MHz a typical spinning rate of 5 kHz is chosen.

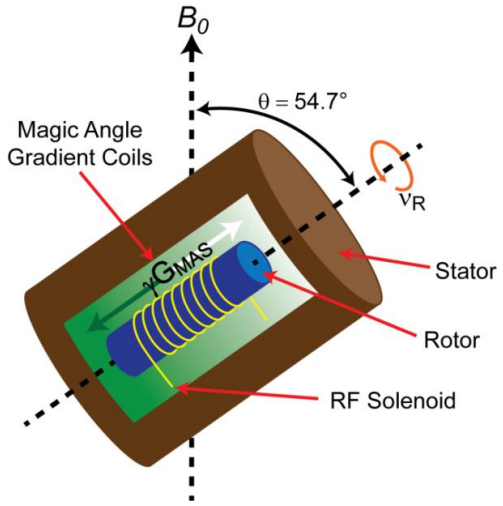

Figure 2.8.4: Schematic of a HR-MAS stator with a magic angle gradient (Alam and Jenkins, 2012; https://www.intechopen.com/books/advanced-aspects-of-spectroscopy/hr-mas-nmr-spectroscopy-in-material-science).

2.8.6. Water suppression

NMR samples for metabolomics studies are usually measured in H_2O for reasons of optimum solubility. The extremely intense water signal of 110 M of water protons in an

aqueous solution gives rise to dynamic range problems and it masks other signals of the sample because of its high linewidth. For these reasons, the water signal has to be removed from the spectrum by a water suppression technique. For the experiments in this thesis the presaturation technique was applied: The frequency of the pulse transmitter is set exactly on the water resonance and a long, weak pulse is applied, which serves to establish equal populations of the two energy levels of the water magnetization and extinguishes the water signal in this way.

2.8.7 The tools and inserts used in HR-MAS-NMR spectroscopy

Various types of inserts are commercially available for HR-MAS samples. These inserts are developed to provide a tight seal that prevents dehydration or even loss of the liquid during the MAS measurements. The inserts used in MAS experiments always depend on the size of the sample, for instance a standard rotor of 4 mm diameter can take 50 µL of sample volume. For 12 µL samples, an insert has to be used. Inserts of different sizes and shapes are available; they have a bottom spacer and a top spacer with a seal screw. The top spacer contains a small hole at the top. When placed into the rotor at the measured distance, any additional will leak through this hole.

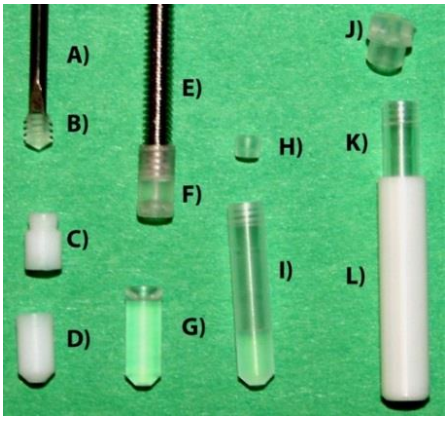

Figure 2.8.5: The tools and inserts used for HR-MAS NMR (Alam and Jenkins, 2012).

In figure 2.8.5. **A**) the specialized Tool for screw cap Insertion, **B**) the sealing screw cap, **C**) the upper Teflon insert, **D**) lower Teflon insert for 30µL volume, **E**) screw for insertion

of the top insert. **F**) Top Kel-F insert, **G**) bottom Kel-F insert of the cap**, H**) plug for disposable insert, **I)** disposable 30µL Kel-F insert, **J)** rotor cap, **K)** disposable insert introduced partially in a 4 mm rotor, **L**) 4 mm zirconia MAS Rotor. All these parts are provided by the BRUKER HR-MAS system.

2.8.8. One-dimensional NMR

The information that can be taken from a ^{1}H NMR spectrum is the chemical shift, which gives information on the chemical environment of a nucleus due to differences in the electronic density around it. Another parameter is the coupling constant, which describes the influence of neighbor nuclei on the nucleus being observed. This effect yields additional structural information, as the couplings give rise to characteristic splittings of the signals into multiplets. An important parameter is also the area under a ^{1}H NMR signal, as it is proportional to the concentration of that nucleus in the sample, i.e. ^{1}H NMR is a quantitative technique.

2.8.9. Spin echoes

Signals of small and large molecules can easily be distinguished in NMR by evaluating the linewidth of the corresponding signal: While ^{1}H nuclei in large molecules lose their magnetization rapidly (short T_2 times, broad signals), nuclei in small molecules show a slow decay of their magnetization (long T_2 times, narrow signals). This effect can be exploited to remove the signals of large molecules (like lipids or proteins) from the spectra and to measure just the signals of the metabolites. This can be achieved with a spin echo experiment (CPMG experiment), named by its inventors Carr, Purcell, Meiboom and Gill, which acts as a T_2 filter: Before data acquisition, the experiment employs a delay time, the length of which is chosen to let the fast T_2 relaxation for large molecules to erase their magnetization, while the signals of the slowly relaxing small molecules are almost not affected.

2.8.10. Two dimensional NMR (TOCSY).

The assignment of the signals in the NMR spectrum to certain metabolites can be a difficult task, especially because of the occurrence of superpositions of signals from different metabolites. Two-dimensional NMR techniques can help in the assignment. These techniques introduce a second frequency axis orthogonal to the first one. In this way, signals being superimposed in the first frequency dimension are most likely to be separated in the second frequency dimension. One two dimensional NMR technique, named TOCSY (Total Coherence Spectroscopy) (Figure 2.8.6), is especially helpful in metabolic analysis, as the signals belonging to a particular metabolite occur along horizontal lines in the spectrum.

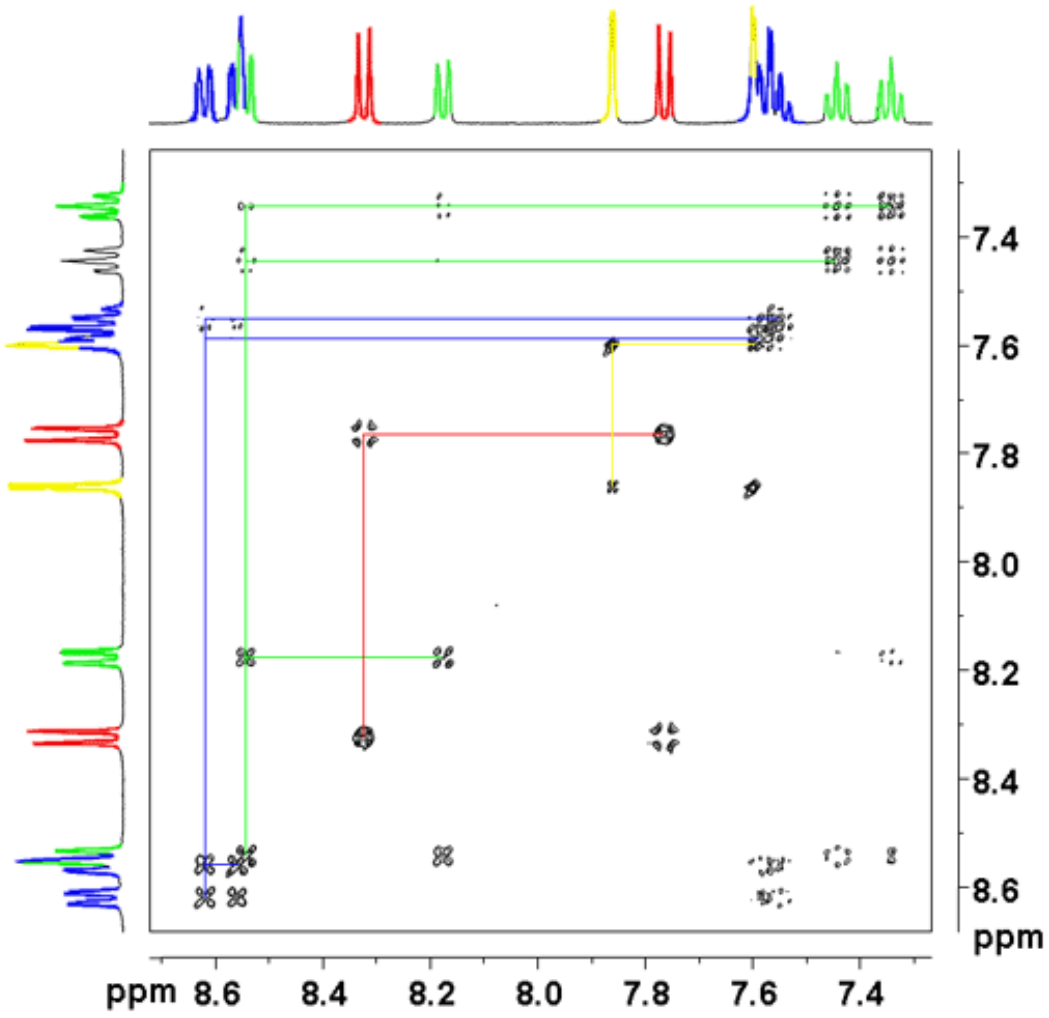

Figure 2.8.6: TOCSY spectrum of a mixture of four metabolites (Source: http://chem.ch.huji.ac.il/nmr/techniques/2d/tocsy/tocsy.html).

MATERIALS AND METHODS

3.1. Animals

To induce acute and chronic toxic liver injuries, male C57BL/6N mice (Javier labs, France), around 8-12 weeks old, were used. The mice were kept under standard conditions and fed *ad libitum* with Sniff R/M-H, 10 mm standard diet (Sniff, Soest, Germany). Another chronic liver disease model used in this study was MDR2-/- mice. This mouse model was developed for periportal liver fibrosis by aging. All protocols for experiments with animals were carried out in full compliance with the help and guidelines from animal care and were approved by the Animal Care Committee of the German government.

3.2. Chemicals

Table 3.2: List of chemicals used in this study.

Chemical	**Company, City-Country**
Bovine albumin fraction (BSA)	SERVA, Heidelberg-Germany
Carbon tetrachloride (CCl_4)	Sigma-Aldrich Crop., Mo-USA
Citric acid monohydrate	Carl-Roth, Karlsruhe-Germany
DAB peroxidase substrate	DAKO, Glostrup-Denmark
Dimethyl Sulphoxide (DMSO)	Sigma- Aldrich Crop., MO-USA
Direct red 80 (Sirius red)	Sigma- Aldrich Crop., MO-USA
Di-Sodium Hydrogen Phosphate Anhydrous	Carl-Roth, Karlsruhe-Germany
Entellan	Merck, Darmstadt-Germany
Eosin-Y (water soluble)	Sigma-Aldrich, Steinheim-Germany
Ethyl alcohol (ethanol)	J.T. Baker, Griesheim-Germany
Fluorpreserve^{TM} reagent	Merck, Darmstadt-Germany
Glycerin	Merck, Darmstadt-Germany
Hydrochloric acid (10MHCl)	Carl-Roth, Karlsruhe-Germany
Hydrogen Peroxide (H_2O_2)	Carl-Roth, Karlsruhe-Germany
Isopropanol (2-propanol, 99.8 %)	Carl-Roth, Karlsruhe-Germany
Ketamine	Ratiopharm, Ulm, Germany

Ly2157299 (Galunisertib)	Gift from Prof. G. Giannelli (Italy)
Mayer's Hematoxylin	Merck, Langenfeld-Germany
Methanol	J.T. Baker, Griesheim-Germany
Olive Oil	Rewe, Germany
Paraffin	Leica Microsys, Wetzlar-Germany
Peroxidase Blocking	DAKO, Glostrup-Denmark
Polyethylene glycol (PEG400)	Sigma-Aldrich, Steinheim-Germany
Picric acid solution	Sigma-Aldrich Crop; Mo-USA
Potassium Chloride (KCl)	Carl-Roth, Karlsruhe-Germany
Potassium di-hydrogen Phosphate (KH_2PO_4)	Carl-Roth, Karlsruhe-Germany
Roti-Histofix 4% (Paraformaldehyde)	Carl-Roth, Karlsruhe-Germany
Roti-Histol	Carl-Roth, Karlsruhe-Germany
Sodium Chloride (NaCl)	Carl-Roth, Karlsruhe-Germany
Normal saline (0.9%)	Braun, Melsungen AG-Germany
Sodium hydrogen phosphate,$Na_2 HPO_4$	Carl-Roth, Karlsruhe-Germany
Sodium hydroxide	Sigma-Aldrich, Steinheim-Germany
TRIS hydroxymetylaminomethane	Carl-Roth, Karlsruhe-Germany
TritonX-100	Carl-Roth, Karlsruhe-Germany
Tween20	Sigma, Schnelldorf-Germany
Weigert´s iron Hematoxylin Kit	Merck, Darmstadt-Germany
Xylazine (2% Rompun)	Bayer, Leverkusen, Germany
Xylene (Dimethylbenzene)	Carl-Roth, Karlsruhe-Germany
Xylene (Dimethylbenzene)	Merck, Darmstadt-Germany

3.3. Equipment

Table 3.3: List of used equipments in this study.

Equipment	Company, City-Country
Analytical Balance BL51S	Sartorius AG, Göttingen-Germany
Bright Field Microscopy (BX 41)	Olympus GmbH, Hamburg-Germany
Centrifuge Rotina 37R	Hettich GmbH, Tuttlingen-Germany
Compact Balance CS200	Carl-Roth, Karlsruhe-Germany
DAKO (Delimiting) Pen	Dackocytomation, Glostrup-Germany
Eppendorf Microtubes (0. 5, 1 and 2 mL)	Sarstedt, Numrecht-Germany
Hybridizer	Dackocytomation, Glostrup-Germany
Incubator	Binder GmbH, Tuttlingen-Germany
Microlance hypodermic needle-26G	BD-Worldwide, Heidelberg-Germany
Microscope Cover Glass	Thermo scientific, Menzel, Braunschweig-Germany
Microscope Slide	Thermo scientific, Menzel, Braunschweig-Germany
Microtome (Microm-HM450)	Microme, Walldorf-Germany
Microwave Oven	Sharpe-Germany
Paraffin embedding cassettes	Carl-Roth, Karlsruhe-Germany
Parafilm	Carl-Roth, Karlsruhe-Germany
pH-Meter (Seven easy PH S20)	VWR GmbH, Berlin-Germany
pH-Electrode blue line 14 pH	Schott Instruments, Mainz-Germany
pH-Meter CG842	Schott Instruments, Mainz-Germany
Pipette, div.	Eppendorf, Wesseling-Berzdorf-Germany
Rotatory shaker Edmund	Buhler, Hechingen-Germany
Tubes (15 and 50mL)	Sarstedt, Nümbrecht-Germany
Water bath JB1	Grant Microsystems, Wetzlar-Germany
Welted glasses	Carl-Roth, Karlsruhe-Germany

3.4. Antibodies and NMR solutions

3.4.1. Antibodies

In Table 3.4.1 descriptions of primary and secondary antibodies, manufacturers and sources are summarized.

Antibody	Raised in	Cat. No.	Company, City-Country
Anti-alpha smooth muscle actin	Rabbit	ab7817	Abcam, Cambridge-UK
Anti-rabbit HRP	Goat	sc-2301	Santa-Cruz, Heidelberg Germany
Anti-pSmad2	Rabbit	CST#3108	Cell Signalling Technology, Frankfurt-Germany
Avidin Biotin Blocking Kit	-	X0590	DAKO, Glostrup-Denmark

3.4.2 Standard solutions for HR-MAS-NMR measurements

Table 3.4.2. Panel of standard chemicals which were used in NMR-based metabolomics.

Chemical	Cat.NO	Company
D_2O	**151882**	**Sigma-Aldrich**
TSP	**269913**	**Sigma-Aldrich**

3.5. Preparation of buffers and reagents

3.5.1 Phosphate buffered saline (stock solution, 10x PBS)

Substances which are used to prepare 10x PBS were included in table 3.3.

Table 3.5.1: 10x PBS buffer preparation.

Substances	Concentration (mmol/L)
Sodium chloride (NaCl)	1370
Potassium chloride (KCl)	27
Potassium Di-hydrogen phosphate (KH_2PO_4)	15
Sodium hydrogen phosphate ($Na_2 HPO_4$)	81
Di-Sodium hydrogen phosphate, anhydrous ($Na_2HPO_4*7H_2O$)	81

Then pH was adjusted to 7.4 and the final volume was brought to 1000 mL with distilled water. In order to prepare 1x PBS: 900 mL distilled water was added to 100 mL 10x PBS and then mixed well.

3.5.2 TRIS-buffer 10x preparation steps

To prepare 1 L TRIS-buffer, the substances in table 3.4 were mixed well.

Table 3.5.2: TRIS-buffer preparation.

Substances	Concentration (mmol/L)
Sodium chloride (NaCl)	137
Potassium chloride (KCl)	2.7
TRIS	25

Then pH was adjusted to 7.4 and the final volume was brought to 1000mL with distilled water. In order to prepare 1x PBS: 900 mL distilled water was added to 100 mL 10x PBS and then mixed well.

3.5.3. Carbon tetrachloride (CCl_4) solution

The toxic dose of carbon tetrachloride (CCl_4) to induce maximal liver damage used in this model was 1.6 g/kg body weight (Hoehme et al., 2010; Zellmer et al. 2010; Hammad et al., 2014) and was prepared as follows: to 3 mL of olive oil, 1 mL of CCl_4 was added and vortexed. All steps of preparation were done under sterile conditions. Dilution of the carbon tetrachloride (CCl_4) was performed under a hood.

3.5.4. Ly2157299 (Galunisertib) solution

To prepare 150 mg/kg Ly2157299, we dissolve 1g of the inhibitor in 2.67 ml DMSO, 8 ml PEG400, 2.67 ml EtOH 70%, 8 ml saline, 5.3 ml 0.01M HCl and mix well. Then the pH of this mixture was adjusted to 6.0. All steps of preparation were done under sterile conditions. Aliquots were prepared and then stored at -20°C.

3.5.5. Antigen retrieval agent (citric acid monohydrate)

In order to prepare 1000 mL from this reagent, 800 mL of distilled water was placed in a clean and sterile beaker, then 2.1 g of citric acid monohydrate was added. Adjustment of the pH to 6.0 was controlled with a pH-meter. The final volume was adjusted to 1000 mL. Thus, the final concentration is 0.01 M. The benefit of using the antigen retrieval reagent is to improve the availability of antigens via break down of protein cross-links formed by the fixation step of the formalin. This procedure helps to increase the permeability of the liver tissue to antibodies.

3.5.6. Blocking serum

This buffer was used to block unspecific binding in immunohistochemistry. 3% bovine serum albumin (BSA) was prepared as follows: 3 g of protease free bovine albumin fraction V was added to a mixture of 1 mL Tween 20 and 99 mL 1x PBS to obtain the final volume 100 mL. 10 mL aliquots were prepared and then stored at -20°C.

3.5.7. Dilution buffer

This buffer was used to block unspecific binding in immunohistochemistry. 3% bovine serum albumin (BSA) was prepared as follows: 3 g of protease free bovine albumin fraction

V was added to a mixture of 1 mL Tween 20 and 99 mL 1x PBS to obtain the final volume of 100 mL. 10 mL aliquots were prepared and then stored at -20°C.

3.5.8. Standard solution for measuring the metabolites

To measure the levels of different metabolites, 3-(Trimethylsilyl) propionic-2,2,3,3-d4 acid sodium salt (TSP) was used as an internal standard for chemical shift calibration and quantification. TSP was dissolved in D_2O to have a reference solution of known concentration.

3.6 Methods

3.6.1 Toxic model for liver fibrosis induction

Chronic liver damage was induced by repeated injections of carbon tetrachloride (CCl_4) for 6 weeks (Yamada and Fausto, 1998; Krizhanovsky et al., 2008; Domenicali et al., 2009, Nussler et al., 2014; Ding et al., 2014). Two doses of 1.6 g/kg CCl_4 were administered intraperitoneally weekly (Figure 3.1.). The application volume of olive oil dissolved CCl_4 was 4 ml/kg. Subsequently, two days after the indicated time point the mice were anesthetized intraperitoneally using a mixture of ketamine (100 mg/kg) / xylazine (2% rompun; 40mg/kg) and both blood and livers were harvested. Litter mates received the same dose of olive oil and served as controls. Three to four mice were used for each group given in the results chapter. Animal application is approved by the Animal Care Committee of the German government (Regierungspräsidium Karlsruhe, application number:35-9185.81/G-216/16).

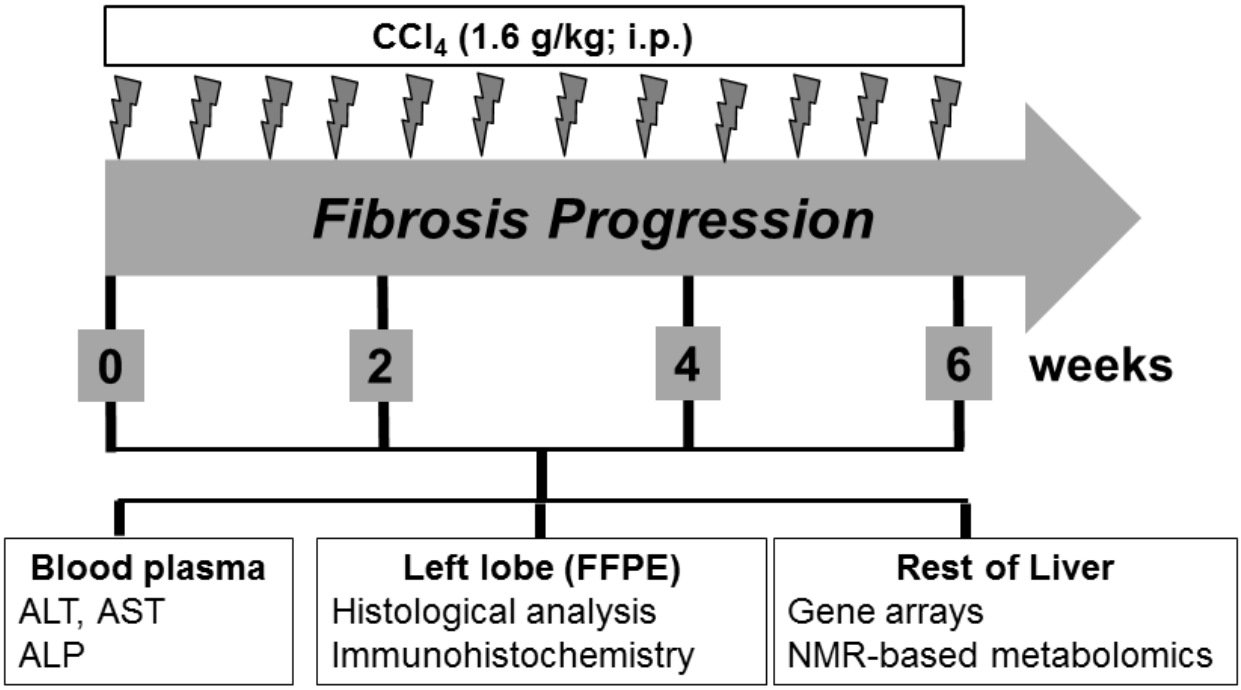

Figure 3.1: Liver fibrosis was induced by repeated intraperitoneal administrations of CCl_4 for 6 weeks. 3-4 mice were analyzed in each group.

3.6.2 Acute liver intoxication using CCl_4

Acute liver injury was induced by a single application of CCl_4 (Hammad et al., 2014; 2017). The material of this section was extracted from our submitted data (Figure 3.2; Hammad et al., 2017). Similarly, two days later the mice were anesthetized intraperitoneally using a mixture of ketamine (100mg/kg)/xylazine (2% rompun; 40mg/kg) and both blood and livers were harvested. Litter mates received the same dose of ethanol and olive oil and served as controls. Three to four mice were used for each group given in the results chapter. Animal application is approved by the Animal Care Committee of the German government (LANUV NRW, application number:8.87-54.04.20.09.325).

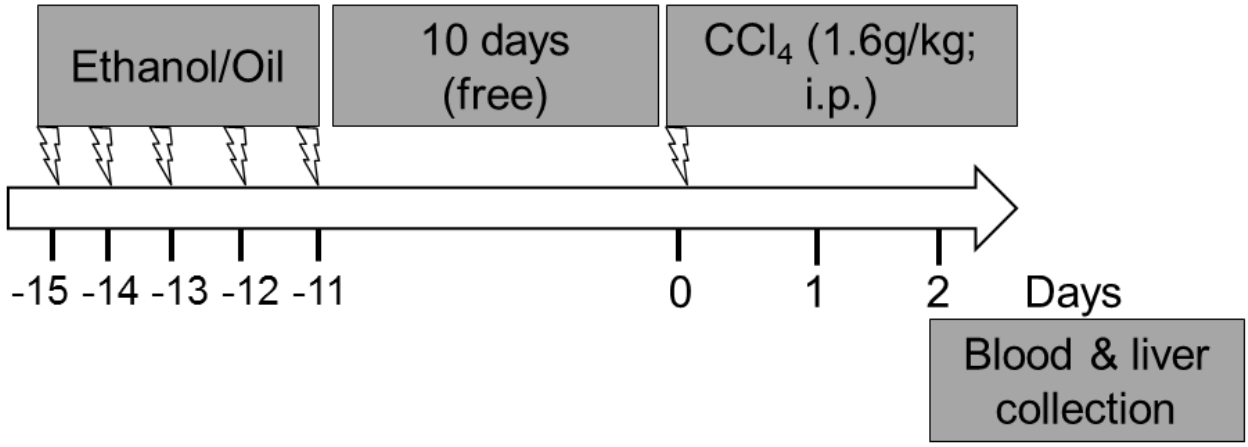

Figure 3.2: Induction of acute liver injury was performed by a single intraperitoneal administration of CCl_4. Five mice were analyzed in each group. The data of this experiment was presented in GASL2017 (Othman et al., 2017) and summarized by Hammad S, Othman A, et al. (2018; Archives of Toxicology-In Revision).

3.6.3 Liver fibrosis in MDR2-/- mouse model

As a rescue experiment, 6 months old MDR2-/- mice were treated with Ly2157299 (Galunisertib; ALK5 inhibitor). ALK5 (TGFβ type I receptor kinase) was used to interfere with TGFβ signaling (Dituri et al., 2013; Giannelli et al., 2014; 2016; Zhang et al., 2014; Herbertz et al., 2015) in MDR2-/- mice. Two groups of mice were used. Ly2157299 treated mice for 14 consecutive days (150 mg/kg) orally. The vehicle treated group received the same amount for 14 days orally. Two days after the last injection, the mice were anesthetized using a CO_2 chamber; then both blood and livers were harvested. Three to four mice were used for each group and for each gender given in the results chapter. Animal application is approved by the Animal Care Committee of the German government (Regierungspräsidium Karlsruhe, application number:35-9185.81/G-172/15).

3.6.4 Excision and fixation protocol of mice liver lobes

At the indicated time point, the mice were anesthetized. After laparotomy, the abdominal cavity was exposed carefully. Then the blood was collected by heart puncture. Subsequently, the liver was excised and the tissue separated into two parts. The first one

was stored in 4% paraformaldehyde (PFA) for embedding in paraffin. The second part was preserved in 4% PFA for only three days followed by a special buffer which is used for preserving the tissue for a long time, this buffer consists of 2% paraformaldehyde and 15% glucose (Hammad et al., 2014).

3.6.5 Protocol of embedding the liver tissue on paraffin

The paraffin cassettes were prepared and cleaned. Then the left lobe of the liver was collected and preserved inside the paraffin embedding cassettes for 48 hours at 4°C. The liver specimens fixed in the formalin were washed by using 1x PBS buffer and a dehydration step was performed with a series of ethanol concentrations according to the following protocol: (Three times, 5 minutes each in 70%, 90%, 95%, and 100% ethanol). The liver specimen were incubated four times in xylene and then overnight in xylene/paraffin (1:1) at 60°. Thereupon, the tissue was incubated twice for three hours in paraffin at 60°C, followed by paraffin embedding at 62°C by using heatable vessels.

3.6.6 Haematoxylin and eosin staining (H&E) staining

The formalin-fixed paraffin embedded liver sections were stained by H&E staining. Haematoxylin and eosin (H&E) staining is one of the most important clinical diagnostic tools and is widely used in medical diagnosis, e.g. to support a pathological analysis of tissue or of a cancer suspected biopsy. The tissue sections were washed three times for 10 minutes each in rotihistol in order to get rid of paraffin, resulting in a total washing time of 30 minutes. Then the tissue sections were rehydrated in different grades of isopropanol (98%, 90%, 80%, 70% and 50%), each for 5 minutes. After the rehydration step the tissue sections were washed in distilled water for 5 minutes, afterwards incubated with Mayer's haematoxylin for 5 minutes and finally washed under running tab water for 20 minutes. Subsequently, the tissue sections were incubated again for three minutes in 4% eosin, then again washed in distilled water to remove the eosin colour. The treatment in graded isopropanol was repeated for 10 seconds per step, and then the tissue sections were washed two times for a few seconds in 100% isopropanol. The tissue sections were again washed

three times in rotihistol and then by using entellan all the sections were mounted. The bright field microscope BX41 was used for inspection.

3.6.7. Protocol of Picro-sirius staining

The embedded paraffin liver sections were stained by using Picro –Sirus red staining as completely described by (Junqueria et al., 1979, Krizhanovsky et al., 2008). The deparaffinization step was performed by washing the liver section three times in rotihistol for 10 minutes each. In order to remove the remaining water, rehydration steps were performed in graded ethanol (70%, 80%, 90%, 95% and 100% ethanol, each step took 10 seconds). Afterwards the liver sections were washed in rotihistol. By using entellan the stained sections were mounted and stored in a cold and dark place until using it for analysis.

3.6.8. pSmad2 immunohistochemistry

The downstream target of TGF-β pathway is Smad phosphorylation; therefore, we used immunostaining of liver sections with antibodies directed against pSmad2 as readout for blocking of this pathway. Briefly, the tissue sections were deparaffinised by using rotihistol three times for 10 minutes each, then the sections were rehydrated by using graded ethanol (100%, 100%, 95%, 90% and 70% ethanol, each for 5 minutes). Subsequently, by using microwaves, the tissue sections were heated in 0.01 M citrate buffer with pH 6.0, twice for 9 minutes each. The incubated sections were cooled down for 30 minutes, followed by a washing step in 1x PBS buffer to remove the remaining buffer. The tissue sections were incubated peroxidase blocking solution for 30 minutes in order to block endogenous peroxidase. All the previous steps were done in a dark and humid place. For blocking the unspecific binding sites, the tissue sections were incubated in 3% BSA/ 0.1% Tween® 20 in 1x PBS for one hour. For blocking the endogenous avidin and biotin, tissue sections were incubated with DAKO kit reagents, following a protocol delivered by the manufacturer. The solution was carefully dripped off (without any washing steps) and the tissue sections were incubated with the primary antibody which is raised in rabbits in a concentration of 1:100 overnight at room temperature. The tissue sections were washed three times in 1x

PBS, each for 5 minutes. Secondary biotinylated antibodies were applied, which are raised in goat 1:250 for 60 minutes at room temperature. After 1 hour incubation the tissue sections were incubated with streptavidin-horseradish peroxidase in a concentration of 1:500 for additional one hour at room temperature. Primary and secondary antibodies as well as streptavidin-horseradish peroxidase were diluted in a blocking serum in (0.3%BSA, 0.1% Tween ® 20 in 1x PBS). The stained tissue was washed with 1x PBS buffer three times each for 5 minutes at room temperature and again incubated with freshly prepared DAB solution for 5 minutes according to the vector lab procedure. Using distilled water the tissue section was rinsed for 5 minutes and then was counterstained using Mayer's haematoxylin for 120 seconds. Afterwards, the tissue section was rinsed again for 10 minutes under running tab-water and then dehydrated by using graded ethanol (50%, 70%, 80%, 90%, 95% and 100% ethanol), each for 10 seconds. The tissue section was again washed in rotihistol. By using entellan the tissue section was mounted and then stored in dark at room temperature until using it for analysis.

3.6.9. Alpha-smooth muscle actin (alpha-SMA) immunohistochemistry

The alpha-smooth muscle actin procedure was performed in order to label the extracellular matrix producing cells (hepatic stellate cells) according to (Krizhanovsky et al., 2008; Hammad et al., 2014) with some modifications. The deparaffinization and rehydration steps were performed as described in section 3.6.8. In order to block the endogenous peroxidase the tissue sections were incubated in a solution of 7.5 % H_2O_2 in methanol for 30 minutes. The tissue sections were washed in 1x PBS buffer three times (5 minutes each). To block the unspecific binding sites inside the tissue, the sections were incubated with 3% BSA, 0.1% Tween ® 20 in 1x PBS for 60 minutes. After that, the endogenous biotin and the avidin blocking were performed by using DAKO recommended protocol. The blocking solution was added carefully to the tissue sections but without washing the sections. The primary antibody used was raised in rabbit (rabbit anti-alpha-SMA, 1:100) for two hours at room temperature. The washing step was done three times (5 minutes each) in 1x PBS buffer. Biotinylated secondary antibody was selected to bind with the primary antibody.

The secondary antibody is raised in goat 1:250, the incubation time was two hours at room temperature. All the experimental steps were done in a humid chamber. The tissue sections were incubated again in streptavidin-horseradish peroxidase with a concentration 1:500 for one hour at room temperature. All the primary and secondary antibodies as well as streptavidin were diluted in a serum with a concentration of 0.3% BSA/ 0.1% Tween®20 in 1x PBS. The stained sections were washed three times (for 5 minutes each) in 1x PBS buffer at room temperature, and the slides were again incubated with freshly prepared DAB solution according to the recommended protocol from Vector lab for 5 minutes until getting the brown colour as a sign of the occurrence of the chemical binding. In order to visualise the nuclei counter staining was performed by using Mayer's haematoxylin for 2 minutes. To get rid of the residual staining, running tab water was used. The sections were stored in a cold and dark place for further analysis.

3.6.10. Liver tissue based quantification

To quantify the necrotic cell area, deposition of extracellular matrix, collagen producing cells and Ly2157299 responding cells, 15 images per liver section of formalin-fixed paraffin embedded liver sections stained with hematoxylin and eosin, picro-sirius red, alpha-SMA and pSmad2 were captured, respectively. The positive areas (Figure 3.6.9) or cells were quantified as a percentage that displays brown staining to the total tested area (15 fields per slide, 10x) using image J or manual counting, respectively.

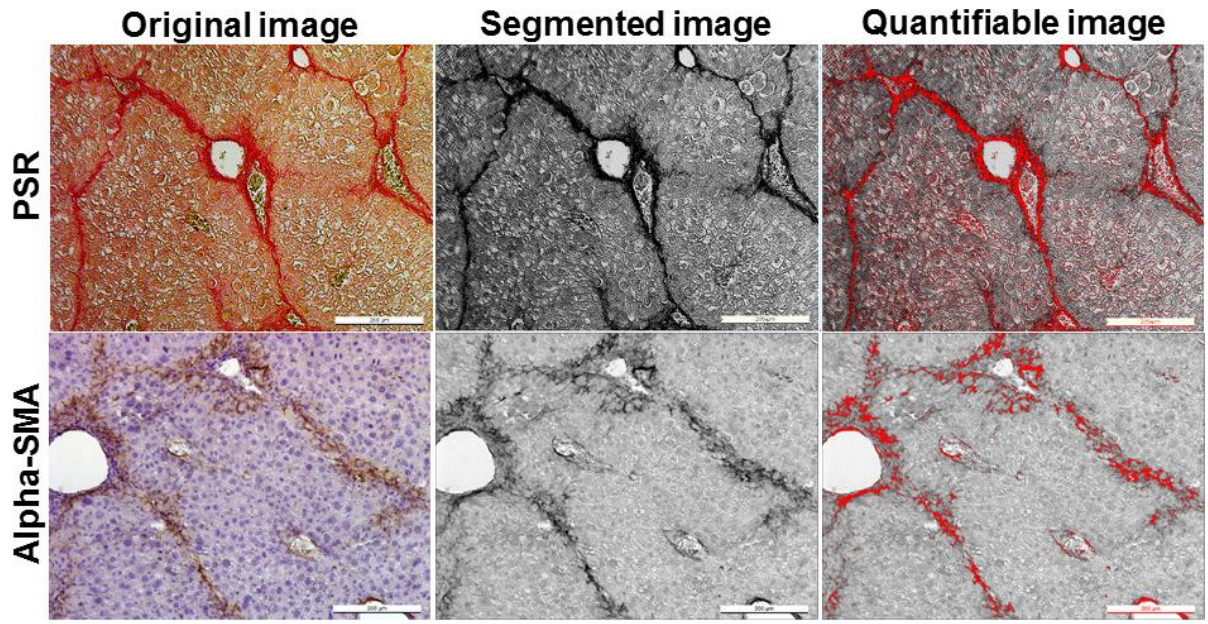

Figure 3.6.9: Pipelines for liver tissue-based quantification of picro-sirius red and α-SMA immunostaining. By using image J, 15 images (10x) were quantified. First, the images were converted to grayscale colored images. Then the threshold of the images was detected manually. Eventually, the colored areas were calculated as a percentage of the whole image. The presented data are mean values ±SE of 4 mice per time point. The same steps were done also to quantify necrotic areas but the areas were manually selected.

3.7. Biochemical analysis

Serum alanine aminotransferase (ALT) and aspartate aminotransferase (AST) levels were determined using analytical kits from Sigma-Aldrich (MAK052 and MAK055, respectively) according to manufacturer's instructions. Other parameters including, alkaline phosphatase, urea, protein, triglycerides and cholesterol were analyzed in core facility (ZMF) at Medical Faculty Mannheim.

3.8. Metabolic quantification from HRMAS-^{1}H-NMR

3.8.1. Sample preparation of liver tissue for HRMAS-^{1}H-NMR.

3.8.2. Metabolite analysis

Metabolomics analysis was performed according to our recently published report (Gogiashvili et al., 2017). It should be noted, that because of the relatively low sensitivity of NMR as compared to mass spectrometry (MS), metabolites having a concentration below the μmolar range cannot usually be detected. For this reason, the number of metabolites found in NMR metabolomics studies usually ranges from 15 to 40. The major advantage of NMR over MS is, however, its noninvasive character: After an NMR measurement of a tissue sample, the RNA integrity number is even large enough to perform a transcriptomics analysis (Gogiashvili et al., 2017).

Moreover, in NMR, the intensities of the signals of different molecules (metabolites) are directly comparable with each other. This is because the signal generation follows the same mechanism, irrespective of the chemical structure of the investigated compounds. This is in sharp contrast to mass spectrometry, where each metabolite requires an individual calibration standard, because the fraction of molecules that arrive at the detector is strongly dependent on their structures. NMR, on the other hand, just requires the calibration of a spectrum with one internal standard: As this standard is inside the sample, it follows the same signal generation mechanism as the metabolites to be detected. So the calibration employed in NMR is inherently quantitative. Hence a validation of the NMR data by using another technique is not necessary.

Preparation for tissue samples: Before sample preparation for NMR analysis, the specimens were stored at -80 °C. The preparation is done under complete humidity exclusion in an atmosphere of nitrogen at -10°C. Dry work conditions are necessary to avoid water condensation on the tissue sample during the preparation process, thus maintaining an exact weight. The low temperature is needed to avoid thawing of the sample, because otherwise the semiliquid consistency of the tissue will impede punching. The tissue is left for 30 minutes and then punched to fit into a disposable insert (DI) container (Bruker,

Rheinstetten, Germany) of 33 µL volume for the 4 mm MAS rotor. The DI is weighed before and after filling in the tissue. The residual volume of the DI is then filled with a 0.3% solution of the sodium salt of deuterated 3-(Trimethylsilyl) propionic-2,2,3,3-d_4 acid (TSP-d_4) in D_2O, which is used to calibrate the spectra. The DI is weighed again and transferred to a 4 mm MAS rotor.

Preparation for blood plasma samples: 60 µL of the blood plasma were pipetted into a 5 mm NMR tube. For technical reasons, the sample volume was increased to 500 µL by addition of D_2O.

NMR measurements of tissue samples: ^{1}H-NMR measurements were performed on a Bruker Avance III 600 spectrometer, operating at 600.35 MHz (14.1 T) for ^{1}H, using the "Magic Angle Spinning" (MAS) technique to eliminate line broadening effects active in heterogeneous samples like tissue. For this purpose, the sample is spun at a frequency of 5 kHz at the "magic angle" of 54.74° with respect to the external magnetic field. All measurements were made at a nominal temperature setting of 276 K. According to a calibration experiment this setting corresponds to a temperature inside the rotor of 4°C. In general, the spinning rate of the HRMAS probe is not fast enough to reduce the linewidth in the case of large molecules, such as proteins and lipids in membranes. To remove the macromolecular background, quantification of metabolites was performed with a spin-echo Carr-Purcell-Meiboom-Gill (CPMG) pulse sequence using a total spin echo delay of 400 ms, i.e. a sequence of 200 π pulses with an evolution time of 1 ms each. 4096 scans were collected over the spectral region of 10 kHz with 16 k time domain data points.

NMR measurements of blood plasma samples: ^{1}H-NMR measurements were performed on a Bruker Avance III 600 spectrometer, operating at 600.35 MHz (14.1 T) for ^{1}H. All measurements were made at a nominal temperature setting of 280 K. Measurements were done with a 5mm HCNP cryogenic probe in order to increase the sensitivity of detection. To remove the macromolecular background, quantification of metabolites was performed with a spin-echo Carr-Purcell-Meiboom-Gill (CPMG) pulse sequence using a total spin echo delay of 400 ms, i.e. a sequence of 200 π pulses with an evolution time of 1 ms each.

1024 scans were collected over the spectral region of 10 kHz with 16 k time domain data points.

Data analysis for the NMR measurements of tissue samples: The resulting free induction decays were Fourier transformed, baseline and phase corrected as well as referenced to the TSP signal using TOPSPIN 3.2 (BRUKER BioSpin GmbH, Germany) software. The TSP concentration in the samples was determined using the "Electronic REference To access In vivo Concentrations" (ERETIC) technique. ERETIC uses an electronic signal as a signal intensity reference for the determination of sample concentrations. The ERETIC signal was generated by a radiofrequency amplifier and is fed into the ^{13}C coil of the NMR probehead. ERETIC was calibrated using a 0.3% sample of TSP-d_4 in D_2O, which is run under identical conditions as the tissue samples. The spectra were then transferred to the Chenomx 7.6 (Edmonton, Alberta, Canada) software, which fits subspectra of the individual metabolites to the measured spectrum. Chenomx was employed both to assign the metabolite signals and to determine the corresponding metabolite concentrations, relative to the TSP concentration, as determined by ERETIC. The resulting relative concentrations were used to calculate tissue concentrations (µmole / g tissue) as follows:

$$\text{Metabolite concentration } \left(\frac{\mu\text{mole}}{\text{g}}\right) = \frac{\text{Mass\_TSP\_solution(mg)} \times 0.003}{(172.23\,\text{g/mol})}$$

$$\times \frac{\text{Metabolite peak concentration Chenomx (mM)}}{\text{TSP peak concentration ERETIC (mM)}} \times \frac{10^6}{\text{Mass of the tissue (mg)}}$$

Data analysis for the NMR measurements of blood plasma samples: The resulting free induction decays were Fourier transformed, baseline and phase corrected as well as referenced to the formic acid signal using TOPSPIN 3.2 (BRUKER BioSpin GmbH, Germany) software. The formic acid concentrations in the samples were determined using the ERETIC technique. ERETIC was calibrated using a 2 mmol sample of sucrose in 90% H_2O/10% D_2O, which was run under identical conditions as the blood plasma samples. The

spectra were then transferred to the Chenomx 7.6 (Edmonton, Alberta, Canada) software, which fits subspectra of the individual metabolites to the measured spectrum. The formic acid concentrations were used as a calibration standard for metabolite concentration determination in Chenomx.

3.9. Statistical analyses

Results are presented as mean ± S.D. When appropriate, Student's t-test or Mann–Whitney's test were used. Statistical significance is indicated as follows: ****$p<0.0001$, ***$p<0.001$, **$p<0.01$, and *$p<0.05$.

RESULTS

Three experiments are included in the result section:

4.1. Liver tissue based metabolic profiling after acute CCl_4 challenge;

4.2. Blood-based metabolites as good biomarkers for CCl_4-induced liver fibrosis;

4.3. Validation of blood-based metabolites in the biliary fibrosis model after ALK5 targeting to rescue disease progression.

4.1. Liver tissue based metabolic profiling after acute CCl_4 challenge

4.1.1. Hepatotoxicity induced by one hit CCl_4

In the first step I tested whether I will be able to quantify the metabolite levels in liver tissues. As part of a submitted manuscript (Hammad S, **Othman A** el al. (2018; Archives of Toxicology-In Revision).), the mice were treated as described in the method section. Figure 1shows routine parameters measured to explore the liver toxicity after acute CCl_4 challenge. The liver to body ratio revealed a significant increase in the intoxicated livers compared to untreated controls (Figure 4.1.1A). However, ALT and AST levels showed dramatic (approximately 125 fold) elevation (Figure 4.1.1B and C) in the intoxicated livers and no change in veh exposed livers. In agreement with transaminases, a necrotic index analysis using image J for HE quantification (Figure 4.1.1D and E) indicated that a necroinflammatory process in the CCl_4 exposed mice was observed. This means that CCl_4 induces hepatotoxicity and at day 2 after the challenge several blood- and tissue-based parameters are significantly altered.

4.1.2. **Tissue based metabolic profiling after one hit CCl_4**

After one CCl_4 hit, I was able to quantify 28 metabolites, namely glutathione, fumarate, leucine, alanine, adenine, methionine, isoleucine, glutamate, betaine, creatine, taurine, trimethylamine, sn-glycero-3-phosphocholine, ascorbate, lactate, threonine, asparagine, ethanol, choline, glutamine, tyrosine, valine, lysine, glucose, o-phosphocholine, phenylalanine and acetate in liver tissues. Figure 4.1.2 shows a heat map of fold changes for the levels of these metabolites in CCl_4 and vehicle exposed livers compared to the average of untreated ones. Only the glutathione level was significantly increased in the intoxicated livers compared to the vehicle group. However, most of the metabolites were either increased or decreased, but not significantly. This could be explained by the analyzed time point: Day two after intoxication is considered a regenerative phase.

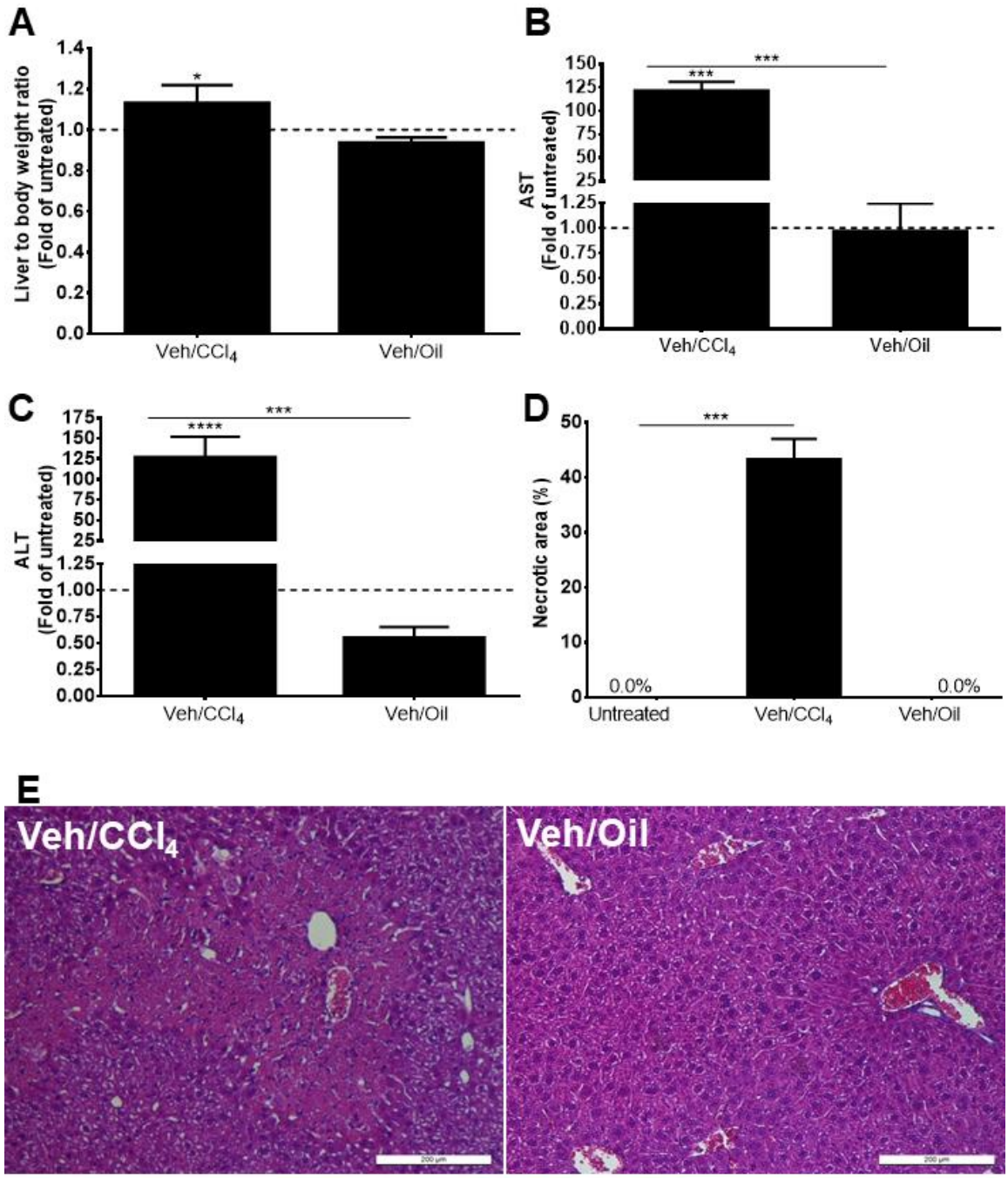

Figure 4.1.1. CCl_4-induced acute liver damage. A) Liver weight as a ratio of mouse weight after CCl_4 or vehicle administration normalized to untreated livers. B and C) Liver transaminases, namely ALT and AST, respectively. D and E) The necrotic index was quantified from HE staining using Image J. The data are mean value ±SE of 3-5 mice per time point. The scale bars are 200µm. the statistical significance is indicated as follows: ****$p<0.0001$, ***$p<0.001$ and *$p<0.05$.

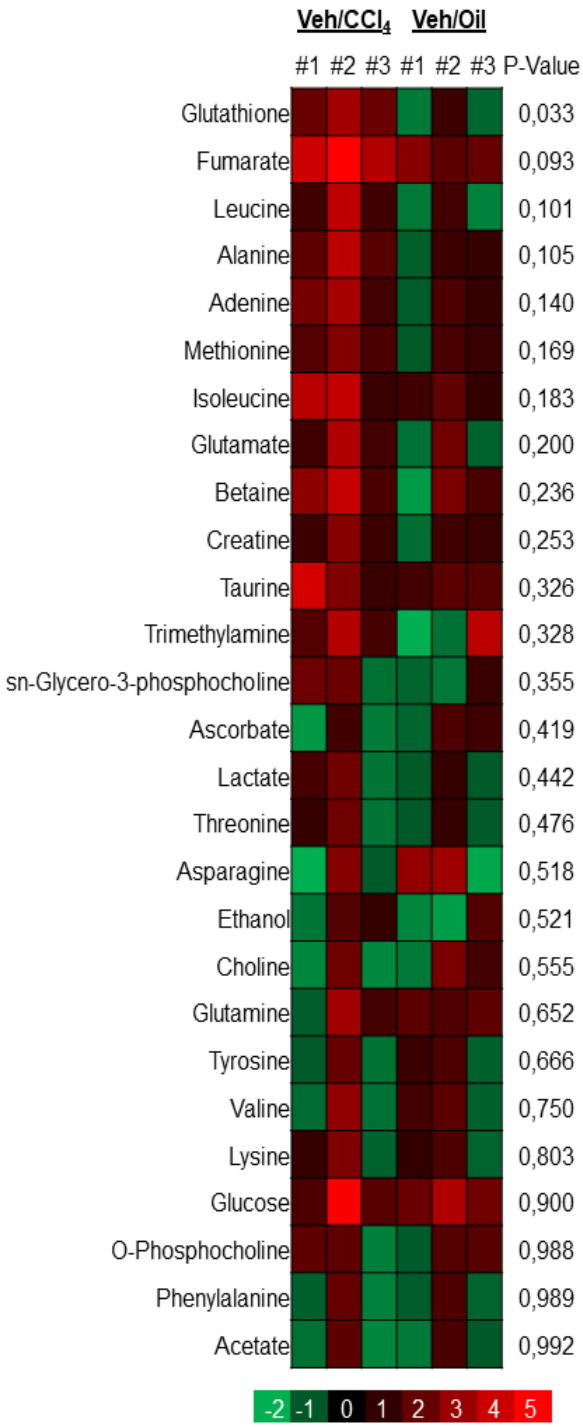

Figure 4.1.2. Liver tissue based metabolic profiling after CCl_4-induced acute damage. The levels of metabolites in 3 mice per group were quantified and normalized to untreated mice. The heat map shows the difference in fold change compared to untreated mice. A red colour refers to increased expression, whereas green refers to decreased levels.

4.2. **Blood-based metabolites as good biomarkers for CCl_4-induced liver fibrosis**

In this experiment, I will try to dissect systemically the CCl_4-induced liver fibrosis to identify possible non-invasive biomarkers for disease staging.

4.2.1. **Mouse weight and liver weight**

We start our phenotype characterization by recording mouse and liver weight after chronic administration of CCl_4 as described in figure 4.2.1. No significant differences were observed in chronically treated livers compared to the control group (Figure 4.2.1). However, there is a time-dependent increase (not significant) in liver weight as a percentage of the body weight (Figure 4.2.1C).

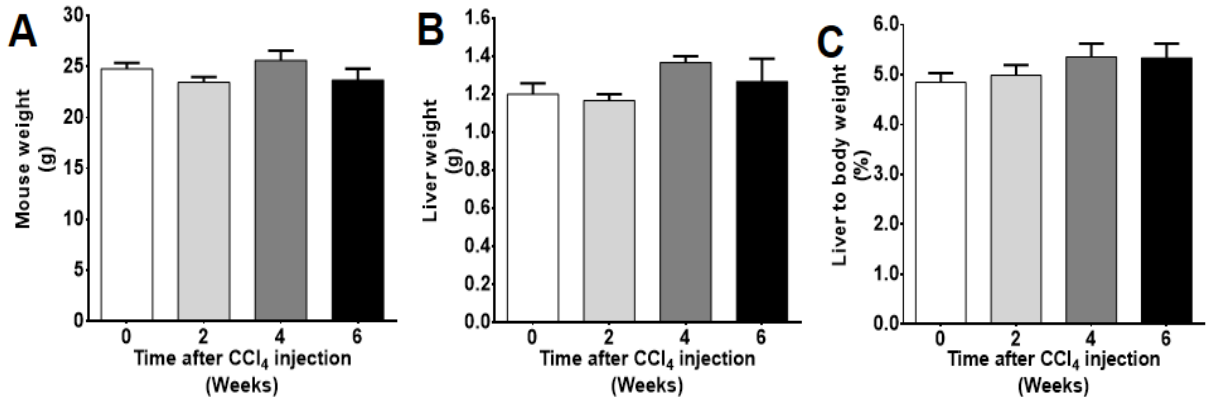

Figure 4.2.1. Mouse and liver weight at different time points after carbon tetrachloride administration. A) Mouse weight. B) Liver weight**. C)** Liver to body weight ration as a percentage. The data are mean value±SE of 3 mice per time point. No significant differences were recorded.

4.2.2. **Blood plasma analysis after chronic liver intoxication**

In the CCl_4-treated mice compared to control, liver damage is reflected by increased plasma alanine transaminase (ALT) and aspartate transaminase (AST) levels (Figure 4.2.2A and B). Expectedly, chronic administration significantly increased the levels of ALT and AST compared to untreated group. In contrast to this finding, the alkaline phosphatase level - a well-known marker for cholangiocyte damage - was not significantly altered (Figure

4.2.2C). Thus, I can conclude that chronic administration of CCl_4 is associated with hepatocyte but not cholangiocyte damage.

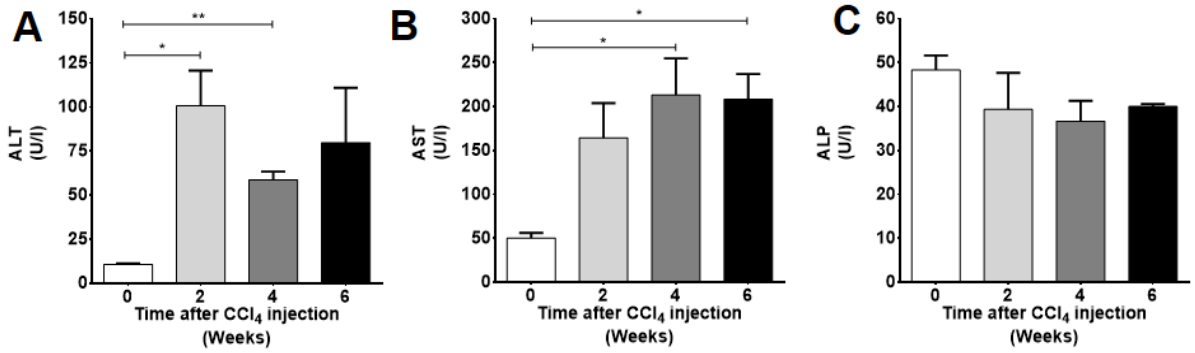

Figure 4.2.2. Liver transaminases and alkaline phosphatase in chronically intoxicated livers. A) ALT. B) AST. **C)** ALP. The data are mean value ±SE of 3 mice per time point. No significant differences were recorded. Statistical significance is indicated as follows: **p<0.01, and *p<0.05.

To investigate, whether chronic administration of CCl_4 affects the level of blood fat substances in the mice, I measured total blood cholesterol and triglyceride. I found no significant changes in both parameters compared to the control group (Figure 4.1.3A). Interestingly, the triglyceride levels in the intoxicated livers increased in a time-dependent manner (Figure 4.2.3A). Furthermore, the urea and the total protein levels are considered a hallmark for kidney efficiency and for ammonia metabolism. In the present study the levels of urea and protein have been assessed in the blood plasma. I found that the urea level is significantly increased (p=0.026) two weeks after CCl_4 injection. Despite the higher levels of urea in the following time points, no significant changes were observed compared to control mice (Figure 4.2.3B). On the other hand, the total protein level is decreased in the blood plasma in a time-dependent manner (not significant), which indicates either a shortage of de novo protein synthesis from liver or an increase of the excretion capacity due to kidney damage (Figure 4.2.3B).

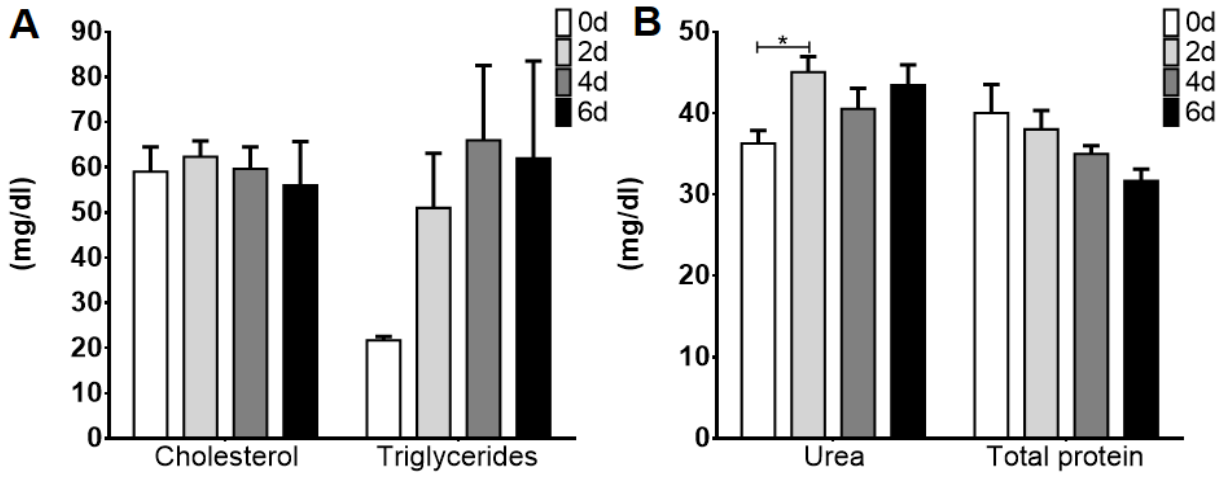

Figure 4.2.3. Blood plasma levels of lipids and protein after chronic administration of CCl_4. The data are mean value±SE of 3 mice per time point. No significant differences were recorded in case of cholesterol **(A),** triglycerides **(A**) and total protein **(B**) compared to the control (0d) group. Statistical significance is indicated as follows: *p<0.05.

4.2.3. **Microscopical analysis**

To visualize the hepatic injury which is represented in the form of hepatocellular necrosis and accumulation of the infiltrated cells occurring in the liver after intoxication with CCl_4, the FFPE sections were stained with haematoxylin and eosin. HE staining indicates that there is hepatocellular injury in the pericentral compartments accompanied with infiltration of small and irregularly shaped nuclei indicated by yellow head arrows (Figure 4.2.4A).

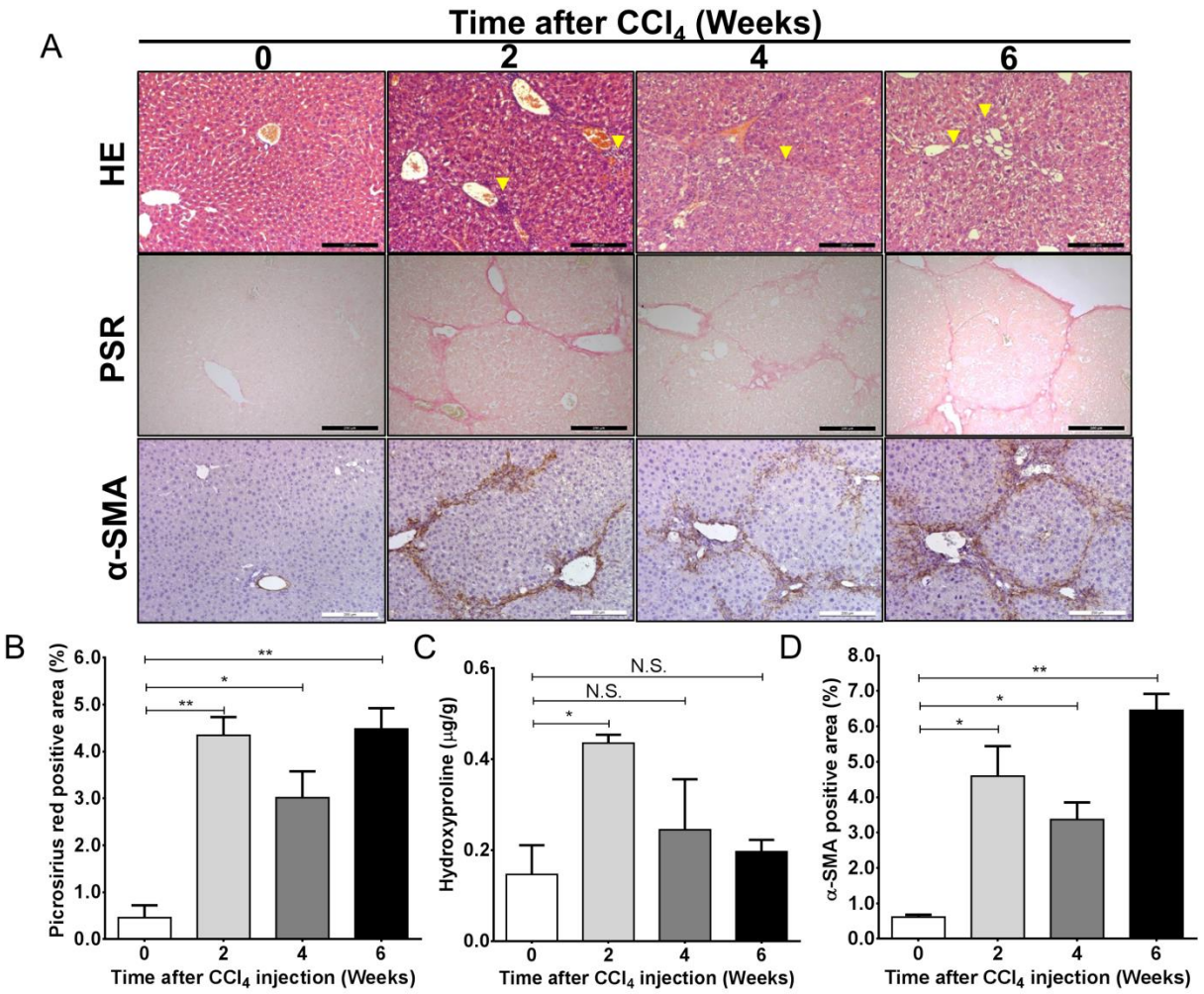

Figure 4.2.4. Standard liver fibrosis characterization with time after CCl_4 administration. A) HE staining revealed numerous infiltrates in fibrotic livers as indicated by yellow head arrows. B) PSR staining was performed to quantify the collagen deposition. C) Hydroxyproline analysis. D) α-SMA was applied to visualize the ECM-producing cells. The data are mean value ± SE of 3 mice per time point. The image analysis was performed using ImageJ. The scale bars are 200 µm. Statistical significance is indicated as follows: **p<0.01, and *p<0.05. HE: hematoxlin&eosin, PSR: picro-sirius red, α-SMA: alpha-smooth muscle actin, ECM: extracellular matrix.

The deposition of extracellular matrix (ECM) and collagen in the treated mice started around the central veins and led to the formation of a bridge between the central veins (Chobert et al; 2012), forming what is called a pseudolobulation (septal fibrosis; Hammad

et al., 2017) as visualized by Sirius red staining (Figure 4.2.4A-B). hydroxyproline levels were determined in liver tissues (Figure 4.2.4.C) indicating that two weeks after CCl_4 higher levels compared with untreated group. The expression of the alpha- smooth muscle actin (α-SMA), which is considered a marker of ECM and collagen producing–cells, was performed by IHC. α-SMA positive expressing cells are defined as activated stellate cells and myofibroblasts (Figure 4.2.4A). The quantification of α-SMA positive area revealed a significant accumulation of the aforementioned cells in fibrotic livers as compared to untreated livers (Figure 4.2.4D). Given in addition to the liver transaminases level, histopathological examination confirmed that this model is suitable to investigate the metabolic profiling aiming to identify consistently altered biomarkers during chronic liver diseases in mice.

4.2.4. **Unfocused liver tissue metabolic profiling**

Using unfocused NMR based-metabolomics, 30 metabolites could be detected in liver tissue. Surprisingly, I observed that 14 out of 30 metabolites were significantly increased two weeks after CCl_4 administration and then decreased to basal levels after 4 and 6 weeks (Figure 4.2.5). Some of these metabolites served as antioxidants e.g. ascorbate, betaine, methionine and tyrosine. This global liver response revealed an adaptation phenomenon (called autoprotection). In the line with this pattern, no further accumulation of ECM with time was recorded.

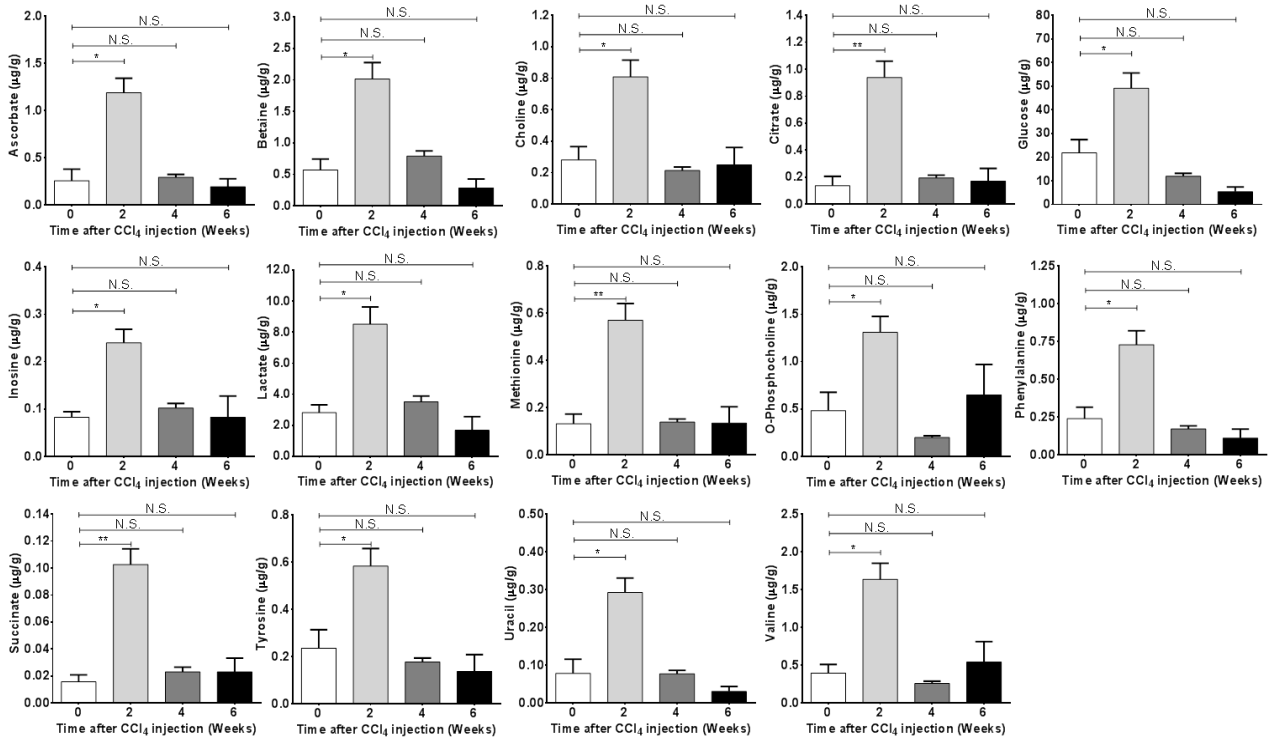

Figure 4.2.5. Unfocused tissue NMR-metabolic profiling as a function of time after CCl_4 injection. These metabolites were significantly altered two weeks after injection and recovered with time. Bars are means ±SE of 3 mice per group. **p<0.01, *p<0.05 and N.S. means non-significant.

In addition to the aforementioned metabolite patterns, 4 out of 30 metabolites, namely isoleucine, leucine, lysine and maleate were significantly altered in two weeks after CCl_4 administration compared to control livers. Non-significant alterations, however, were recorded for other time points (Figure 4.2.5). The levels of these metabolites, that were obtained 6 weeks after injury, showed a dramatic variation between individuals.

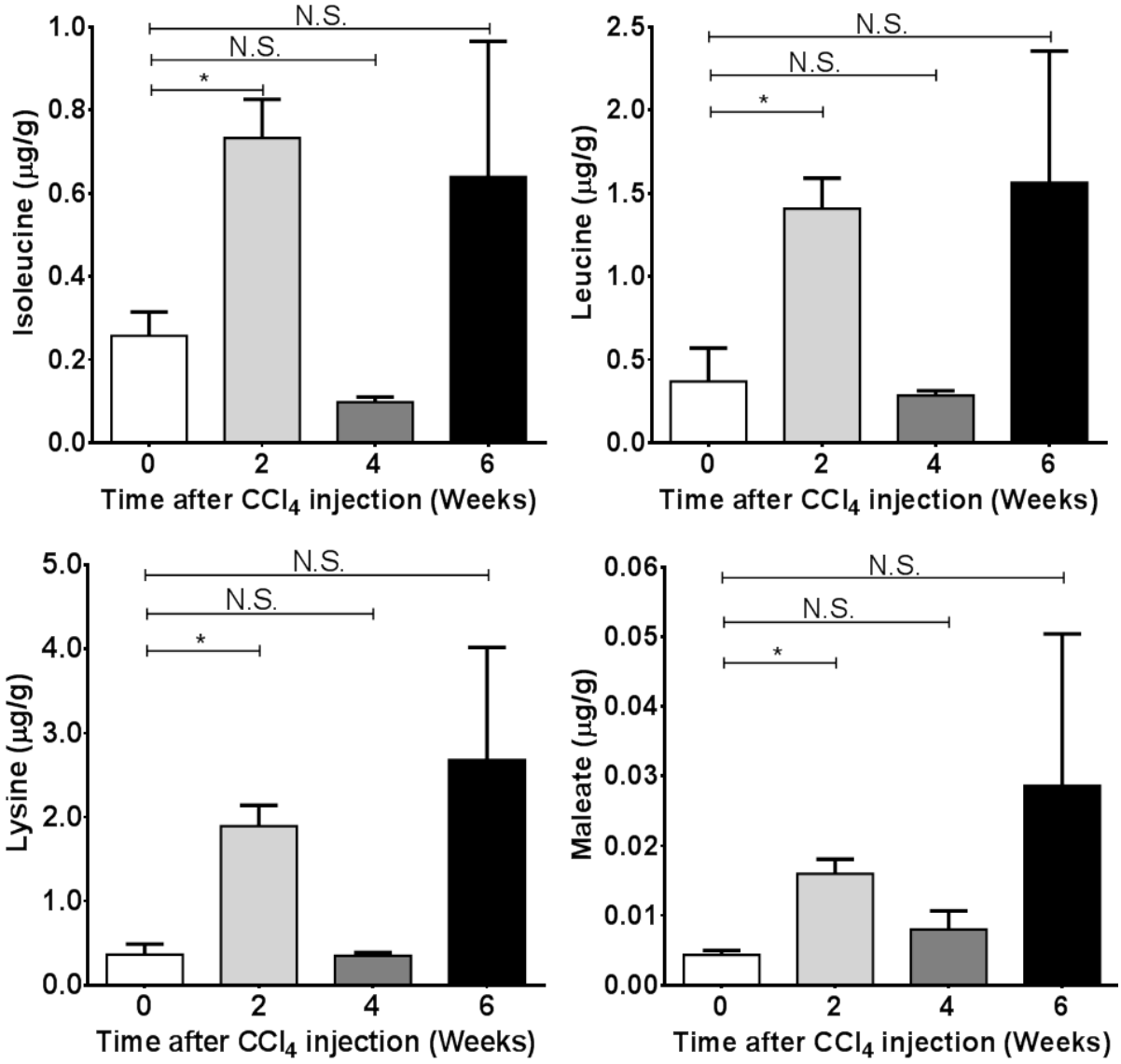

Figure 4.2.6. Unfocused tissue NMR-metabolic profiling as a function of time after CCl_4 injection. These metabolites were significantly altered two weeks after injection and recovered with time, however, dramatic individual variabilities after 6 weeks were observed. Bars are means±SE of 3 mice per group. *p<0.05 and N.S. means non-significant.

In addition to the aforementioned metabolite patterns, 6 out of 30 metabolites, namely adenine, alanine, ethanol, glutamate, niacinamide and taurine were non-significantly altered in fibrotic livers compared to control livers (Figure 4.2.7).

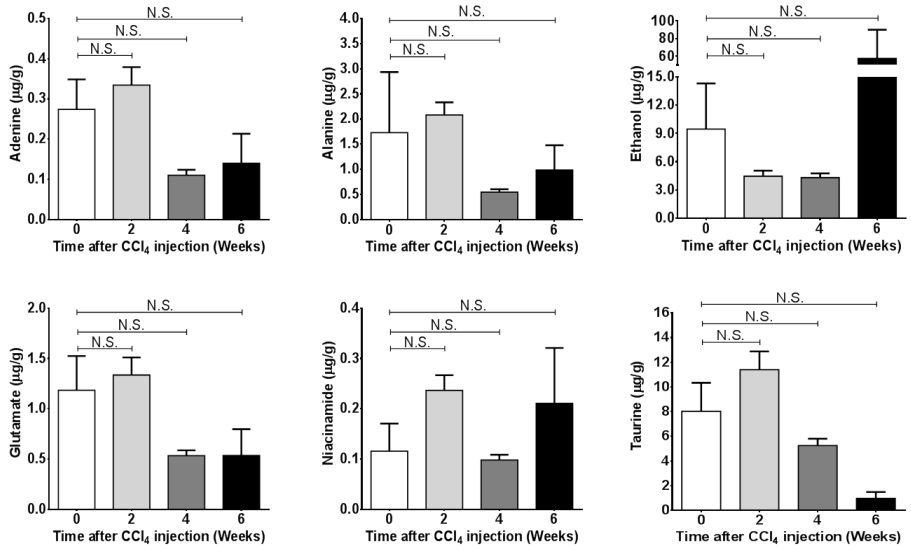

Figure 4.2.7. Unfocused tissue NMR-metabolic profiling as a function of time after CCl_4 injection. Non-significant alteration was recorded. Bars are means±SE of 3 mice per group. N.S. means non-significant.

The following metabolites were affected differently as a function of time after CCl_4 administration, namely acetate, asparagine, butyrate, glutamine, dimethylamine and fumarate (Figure 4.2.8).

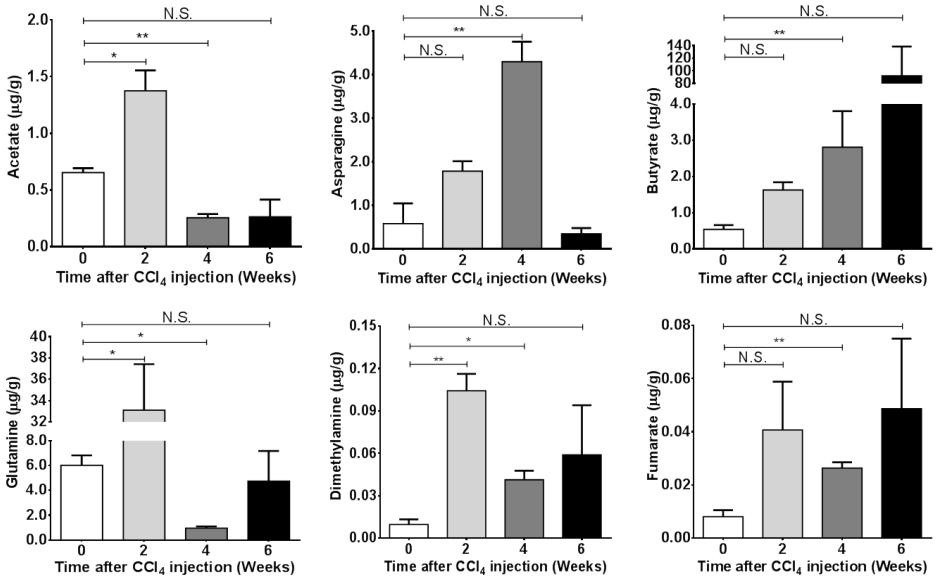

Figure 4.2.8. Unfocused tissue NMR-metabolic profiling as a function of time after CCl_4 injection. Six metabolites were outliers. Bars are means±SE of 3 mice per group. **p<0.01, *p<0.05 and N.S. means non-significant.

4.2.5. **Unfocused metabolic profiling of blood plasma**

Using NMR based-metabolomics 15 metabolites could be determined in the blood plasma of control and fibrotic mice after repeated toxic doses of CCl_4. I was able to cluster the identified metabolites into different categories: i) Metabolites that were expressed in high level during fibrogenesis. This cluster represents the majority. It includes acetate, betaine, citrate, ethanol, glucose, phenylalanine and pyruvate. Among those metabolites only betaine, ethanol, glucose, phenylalanine and pyruvate showed a significant alteration (Figure 4.2.9); ii) Metabolites that were unaltered in fibrotic livers, e.g. alanine, formate and o-phosphocholine (Figure 4.2.10); and iii) The level of valine decreased consistently in fibrotic livers compared to the livers of untreated animals (Figure 4.2.10). Altogether, the first and third clusters are important to identify consistently altered metabolites for further characterization in another animal model as robust blood based biomarkers.

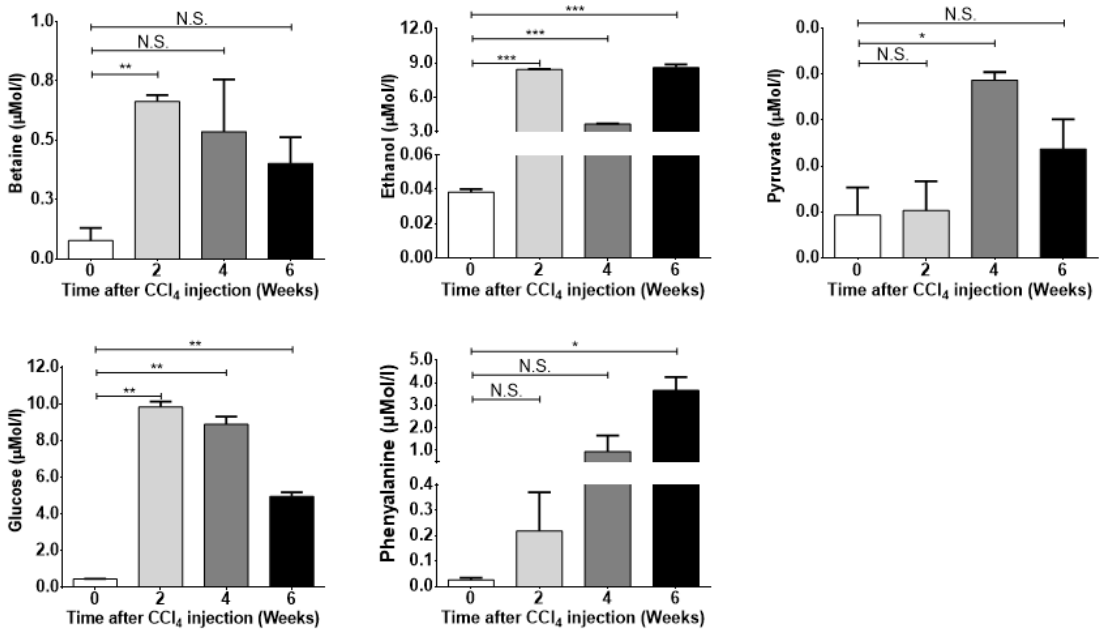

Figure 4.2.9. Metabolic profiling of blood plasma after chronic CCl_4 treatment. Several metabolites as shown were consistently altered in fibrotic livers compared to controls. Statistical significance is indicated as follows: ***p<0.001, **p<0.01, and *p<0.05.

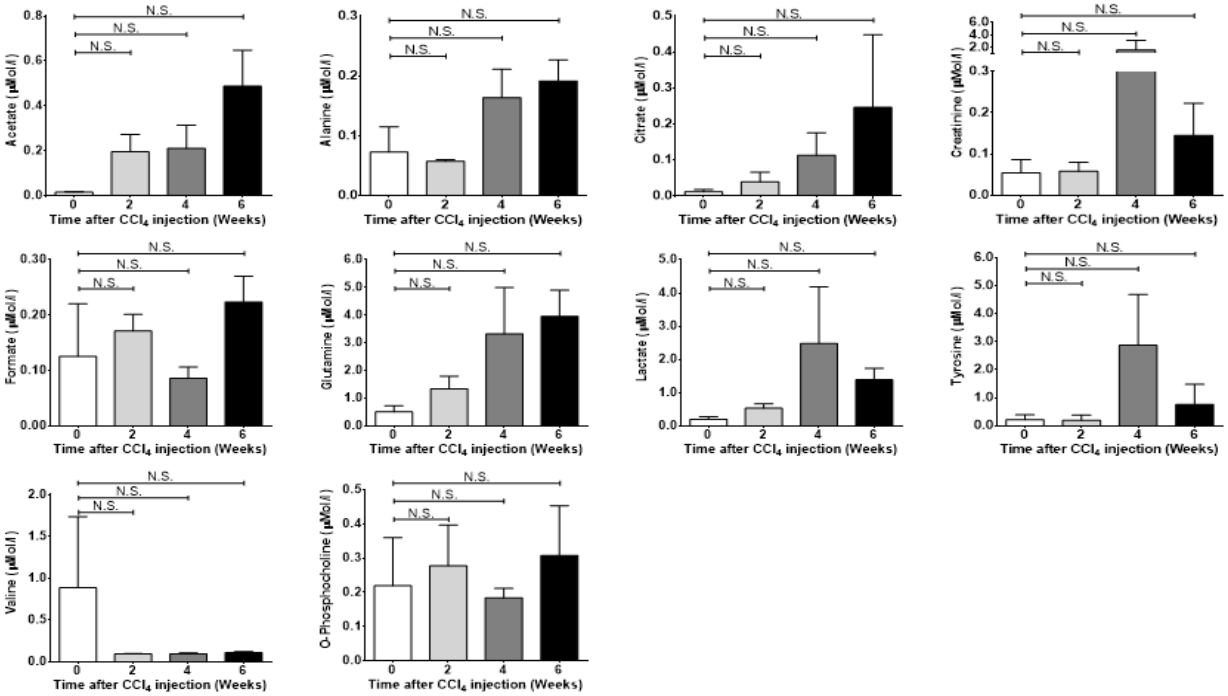

Figure 4.2.10. Non-significantly altered blood plasma metabolites after chronic CCl_4 treatment. The bars are means±SE of 3 mice per group. N.S. means non-significant.

4.2.6. Correlation of deregulated metabolites in blood plasma with standard fibrosis parameters

To further identify possible plasma-based metabolites as biomarkers, I correlated the obtained values from metabolomics for each mouse with clinical and histopathological parameters. Such an approach (Pearson correlation) helped us to exclude those metabolites which do not correlate with standard fibrosis parameters. I found that several metabolites were significantly correlated with ALT or AST levels, e.g. acetate, betaine, ethanol, glucose and phenylalanine. In this line, those metabolites were also positively correlated with tissue-based parameters, e.g. PSR and alpha-SMA. Obviously, most of the tested blood-based metabolites were positively correlated (not significantly) with blood and/or tissue parameters, e.g. alanine, citrate, creatinine, formate, glutamine, o-phosphocholine, phenylalanine, pyruvate and tyrosine. Only the valine level was negatively correlated with blood- or tissue- based parameters.

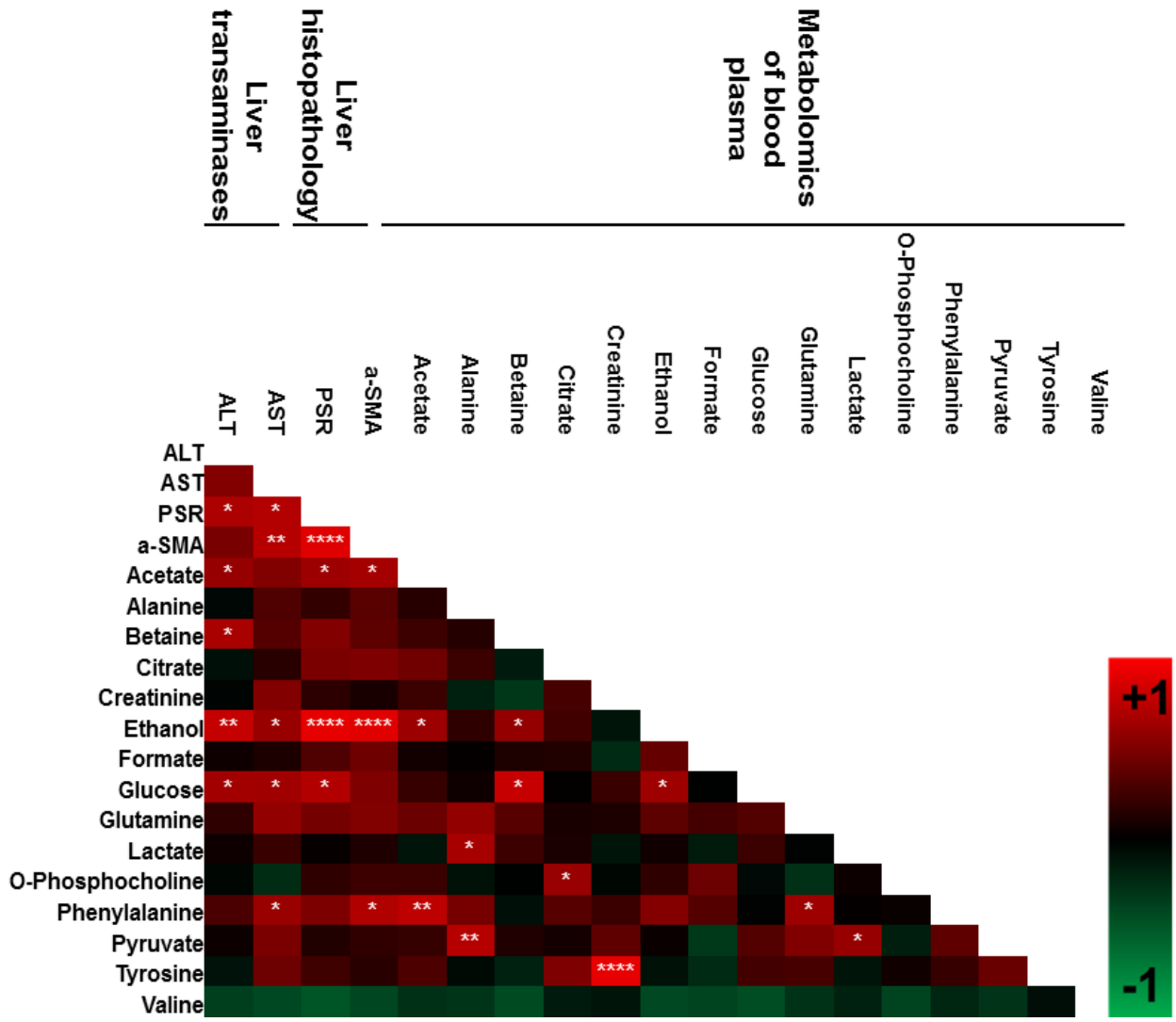

Figure 4.2.11. Metabolic profiling correlation of blood plasma versus clinical data and histopathology. Red and green colors refer to positive and negative correlation, respectively. Three mice per group (0, 2, 4 and 6 weeks after repeated CCl_4 injections) were used in this analysis. The statistical significance is indicated as follows: ****p<0.0001, **p<0.01, and *p<0.05.

4.2.7. **Correlation of the same metabolites in blood and in liver tissue**

In this step, I tried to correlate the levels of the same metabolite in blood and liver tissues. Among the identified metabolites 12 were reported in both context.

In Figure 4.2.12, the heat map shows the correlation coefficient between the same metabolites in blood plasma and liver tissue. Using such an approach (Pearson correlation), it is obvious that most of the identified blood-based metabolites were negatively correlated with tissue levels (Figure 4.2.12). In contrast, betaine, glucose and ethanol were positively correlated. This could be explained by an extrahepatic contribution of most metabolites indicating organ homeostasis.

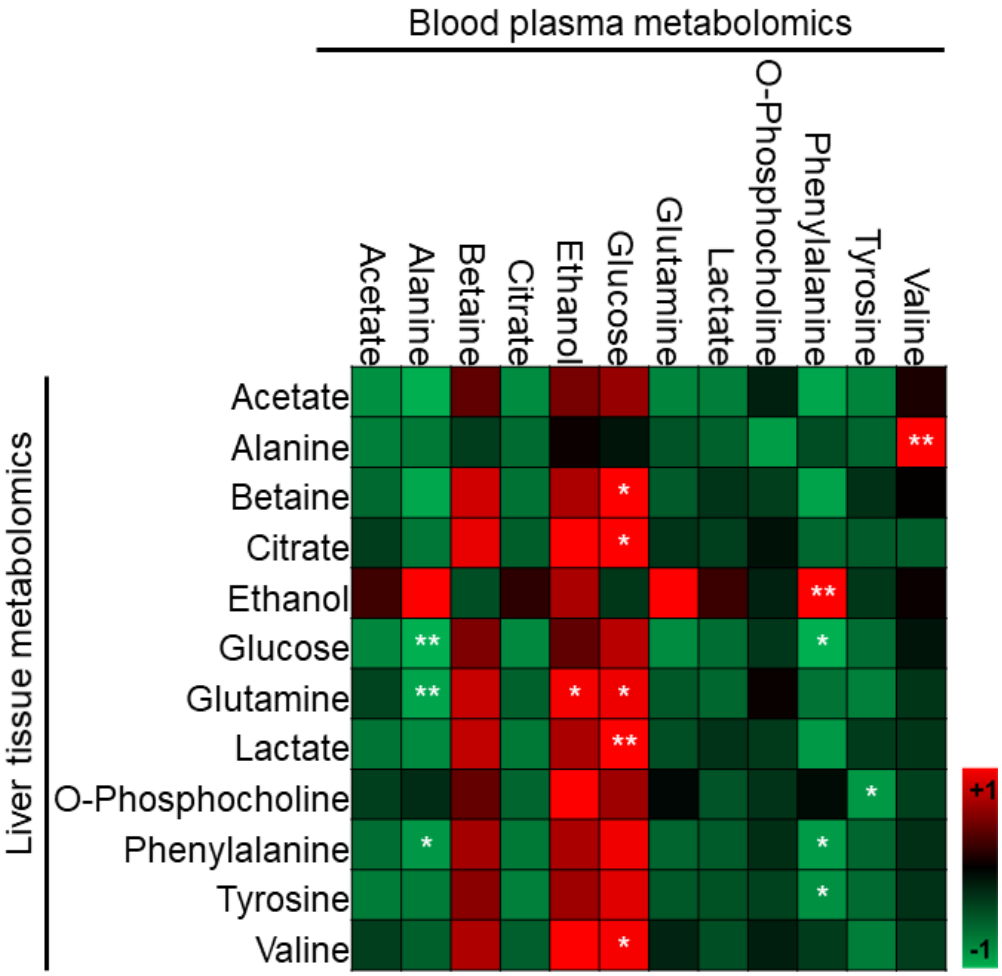

Figure 4.2.12. Metabolic profiling correlation of blood plasma versus liver tissue. The same set of metabolites from the same mouse was evaluated in blood and in liver tissue and correlated. Red and green colors refer to positive and negative correlation, respectively. Three mice per group (0, 2, 4 and 6 weeks after repeated CCl_4 injections) were used in this analysis. The statistical significance is indicated as follows: ****$p<0.0001$, **$p<0.01$, and *$p<0.05$.

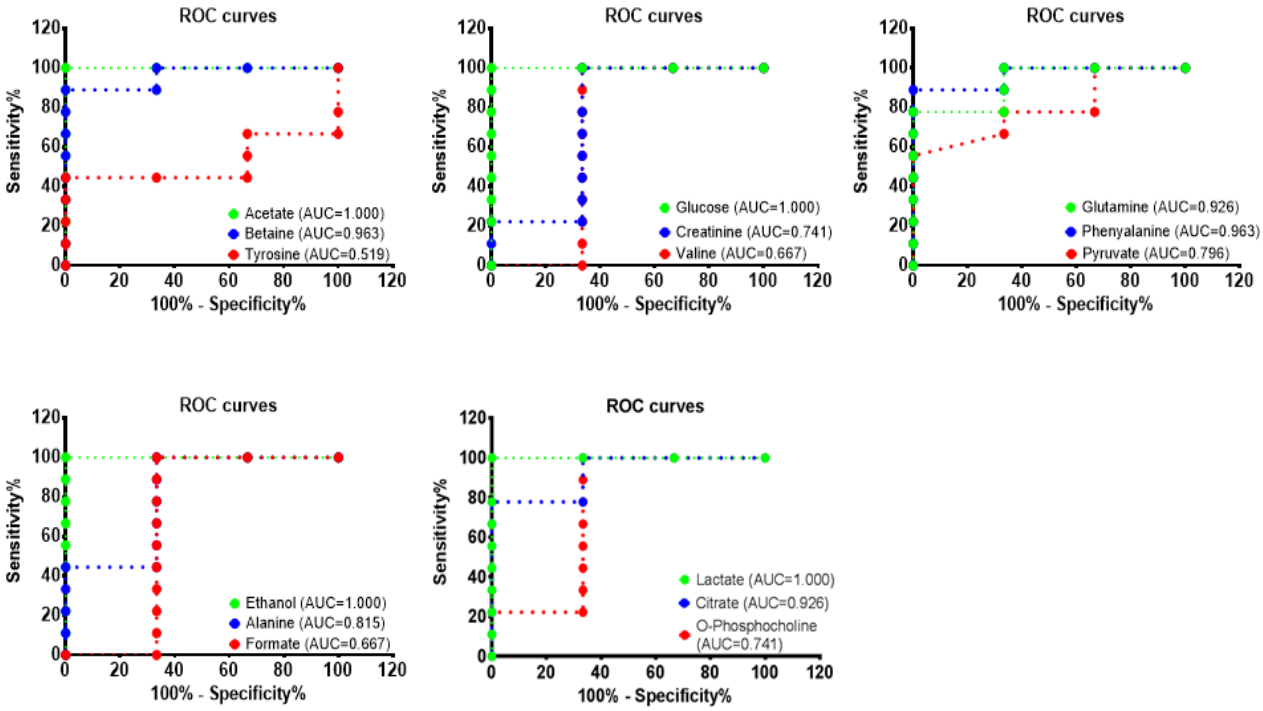

Figure 4.2.13. ROC curves showing the potential of the identified metabolites to distinguish between healthy and fibrotic livers. The AUC value, which denotes area under the curve, for some metabolites, e.g. acetate, glucose, lactate and ethanol, was 1.00, which proves that they are very good biomarkers. Also betaine, phenylalanine, alanine, glutamine and citrate were identified as good biomarkers with an AUC of more than 0.800. However, tyrosine, creatinine, pyruvate, formate and o-phosphocholine were just fair indicators for liver fibrosis and AUC ranged between 0.5 and 0.8. In order to generate the ROC curves, three healthy and untreated animals were compared with nine treated animals (i.e. three groups of three animals each, treated for 2, 4 and 6 weeks after repeated CCl_4 injections).

4.2.8. **Blood based biomarkers for liver fibrosis**

A further step-wise comparison was also carried out between healthy and fibrotic livers to investigate the metabolic perturbation that fibrogenesis brings about. The technique of "Areas under the ROC curves" (AUC) was applied to plot the true positive rate (sensitivity) versus the false positive rate (100% - specificity). Each point on the plotted ROC curve

refers to a sensitivity/specificity pair corresponding to a particular decision threshold (comparing healthy versus fibrotic livers). Using this well-known fundamental tool for diagnostic test evaluation of biomarkers, we were able to evaluate the AUC for 15 blood based metabolites in fibrotic versus healthy livers (Figure 4.2.13, Table 4.2.1). Surprisingly, the AUC values of acetate, glucose, ethanol and lactate were all 1.00, indicating that these metabolites could be applied conclusively to distinguish between healthy and fibrotic livers. In addition, other metabolites, e.g. betaine, glutamine, phenylalanine, alanine and citrate were very good disease indicators where the AUC was more than 0.800. However, the remaining metabolites were fair indicators and this group included tyrosine, creatinine, pyruvate, o-phosphocholine and formate. Blood based metabolic profiling is a powerful tool to identify the potential biomarkers for clinical purposes and to investigate -in depth- fibrogenesis on the molecular level. Further validation of these very good markers (first and second groups) in clinical cohorts will follow in the future study.

Table 4.2.1: Areas under the ROC curves of clinical parameters, histologically based analysis and blood-based metabolites. Red highlighted metabolites were considered very good biomarkers distinguishing healthy from fibrotic livers and the AUC value was more than 0.800. In order to generate the ROC curves, three healthy and untreated animals were compared with nine treated animals (i.e. three groups of three animals each, treated for 2, 4 and 6 weeks after repeated CCl_4 injections).

	Parameters	Area under the curve (AUC)
Blood plasma	ALT	1.000
	AST	1.000
	AAR	0.852
Tissue-based parameters	PSR	1.000
	α-SMA	1.000
NMR-based plasma metabolomics	Acetate	1.000
	Ethanol	1.000
	Glucose	1.000
	Lactate	1.000
	Betaine	0.963
	Phenylalanine	0.963
	Citrate	0.926
	Glutamine	0.926
	Alanine	0.815
	Pyruvate	0.796
	Creatinine	0.741
	O-phosphocholine	0.741
	Formate	0.667
	Valine	0.667
	Tyrosine	0.519

4.3. Validation of blood-based metabolites in the biliary fibrosis model after ALK5 targeting to rescue disease progression.

In order to test the applicability of this technology to evaluate metabolites as disease biomarkers, I quantified the blood plasma from MDR2-/- mice upon transforming growth factor-β1 (TGF-β1) targeting. Currently, targeting the TGF-β1 pathway via a small molecule, Galunisertib, (inhibiting ALK5 intracellularly), and therewith the phosphorylation of Smad2, is already in clinical trials phase II to treat hepatocellular carcinoma patients (NCT02423343). Therefore, in a different animal model based on the genetic manipulation of 6 months old ABCB4 (MDR2-/-) mice exposed to galunisertib (Ly2157299), I tried to evaluate the metabolite levels using the same tool as described in the previous section. Briefly, the ABCB4-/- mice - a well-established model for biliary fibrosis to hepatocellular carcinoma- were treated daily via an oral gavage with Galunisertib (150mg/kg) for 14 consecutive days. Two days after the last dosage, blood plasma and livers were harvested from 6 vehicle- and 6 Ly2157299- exposed mice for further assessments, e.g. ALT, AST, ALP, fibrosis scoring and Smad2 phosphorylation as well as for metabolic profiling and fibrosis scoring.

4.3.1. Mouse and liver weight and hepatic enzymes

No significant changes were observed in the body weight of Ly2157299-exposed mice compared to the vehicle treated group indicating that the experimental setting was not toxic (Figure 4.3.1). Moreover, liver transaminases, namely ALT and AST were slightly reduced in the Ly2157299 mice (Figure 4.3.1). In the same line, alkaline phosphatase (ALP) was slightly reduced in the treated compared to the untreated animals (Figure 4.3.1). This revealed that upon Ly2157299 exposure, the liver functions were slightly (but significantly) improved.

4.3.2. Liver fibrosis is slightly normalized by Ly2157299

A further characterization of this improvement upon Ly2157299 was performed using liver tissue levels. The fibrosis index was significantly reduced ($p<0.05$) as tested by Picro-sirius

red staining (Figure 4.3.2). In addition, pSmad2 immunohistochemistry showed a significant reduction (P<0.01) in the number of labelled hepatocytes upon Galunisertib administration (Figure 4.3.2). These results revealed that Ly2157299 - to some extent - normalized liver fibrosis and further adjustments of the dose and the duration of exposure are required. Further experiments are ongoing to determine which mechanisms could explain the effect of the ALK5 inhibitor in this disease context.

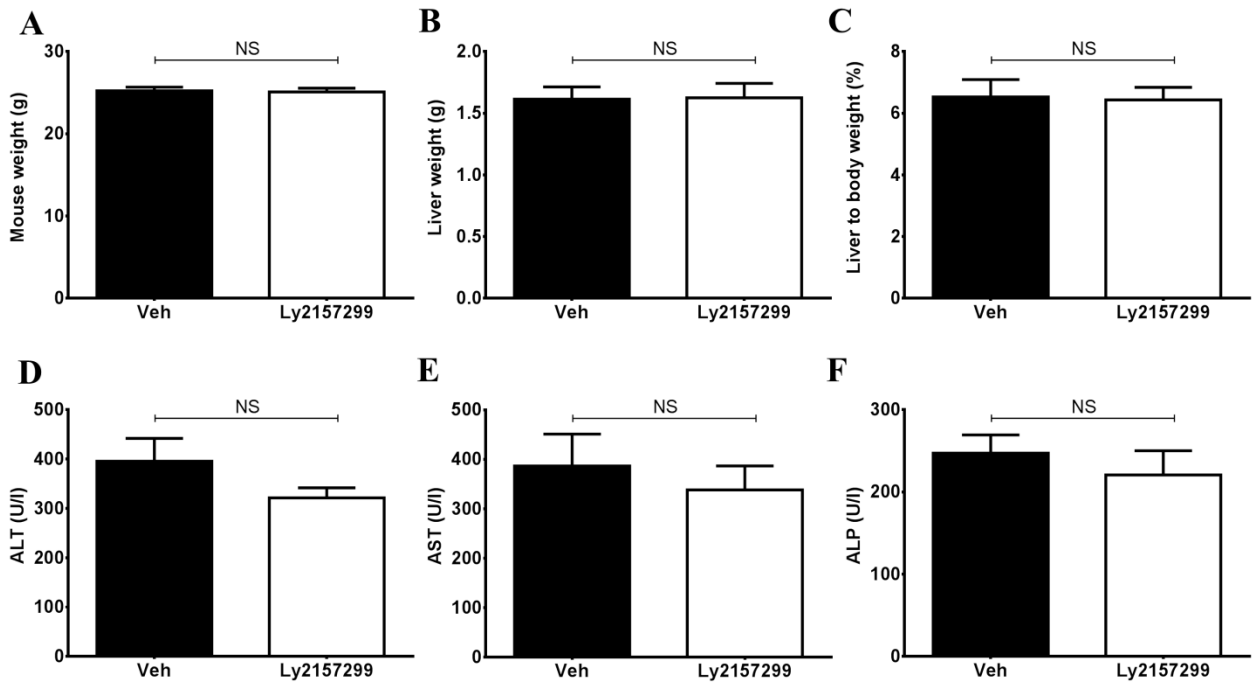

Figure 4.3.1. Mouse and liver weight as well as liver related enzymes upon Ly2157299 and vehicle exposure. A-C) Mouse and liver weight were detected upon Ly2157299 treatment. **D-E**) Liver enzymes namely ALT, AST and ALP. Mouse and liver weight were detected upon Ly2157299 treatment. The data are mean value±SE of 6 mice per group. NS: No significant differences were recorded.

4.3.3. **Blood based metabolic profiling upon Ly2157299 administration**

Using NMR based-metabolomics I was able to determine 23 metabolites (Table 4.3.2) in the blood plasma of vehicle and Ly2157299 exposed mice. Seven out of 23 metabolites, namely formate, lactate, 3-hydroxyisobutyrate, alanine, methionine, tyrosine and acetate were significantly altered upon Ly2157299 exposure compared to vehicle treated mice.

Other metabolites showed non-significant alteration, though some trends were recorded (Table 4.3.2).

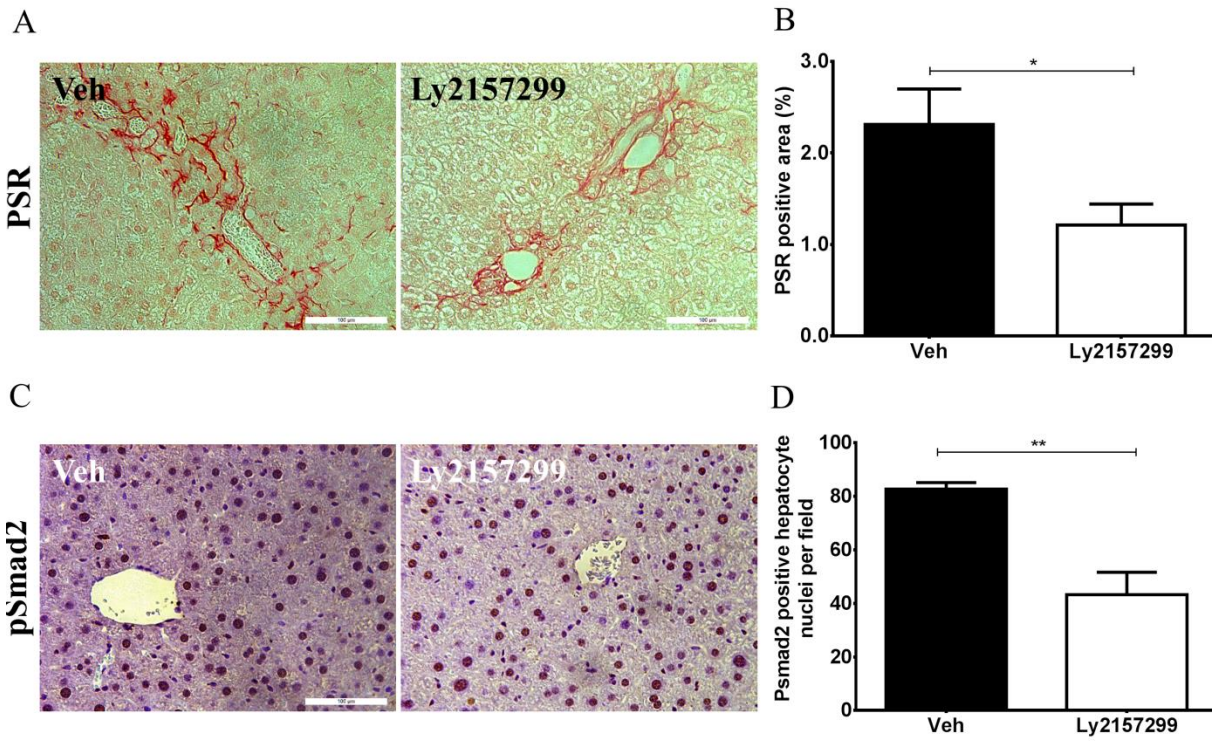

Figure 4.3.2. Standard liver fibrosis characterization and TGF-β1 pathway in vehicle versus Ly2157299 exposed livers. **A-B**) Picro-sirius red (PSR) staining was performed to quantify the collagen deposition. **C-D**) pSmad2 immunohistochemistry revealed a significant reduction in Smad2 phosphorylation. The data are mean value±SE of 6 mice per group. The image analysis was performed by ImageJ. The scale bars are 100 µm. Statistical significance is indicated as follows: **p<0.01, and *p<0.05.

4.3.4. Metabolites altered in both models of fibrosis

Among those metabolites detected in both mouse models (septal fibrosis induced by CCl_4 and ALK5 targeted-biliary fibrosis), several targets were found, e.g. acetate, alanine, formate, glucose, glutamine, lactate and phenylalanine. Lactate, acetate and alanine were considered the best markers for both models. However, the difference between both models could be explained by different liver metabolic zonation of the extracellular matrix, which

in the CCl_4 model was zone III, while in MDR2-/- it was zone I. Therefore, from the septal CCl_4-induced fibrosis model I can conclude that betaine, citrate, glutamine and phenylalanine should be tested in clinical cohorts. However, in biliary fibrosis, 3-hydroxyisobutyrate, formate, glutamate, glycine, methionine and tyrosine should be tested in clinical cohorts instead.

Table 4.3.2: Average levels of metabolites (µmol/l±SD) from Ly2157229 and vehicle exposed mice. Red highlighted metabolites were considered very good biomarkers distinguishing healthy from fibrotic livers and AUC was more than 0.7900. Six vehicle exposed mice (diseased group) were compared with 6 animals treated with Ly2157299 (treated group) to calculate AUC.

	Ly2157229±SD	Veh±SD	P-Value	Area under the curve (AUC)
Formate	0.062±0.003	0.023±0.016	0.0002	1.000
Lactate	0.065±0.002	0.388±0.305	0.0269	1.000
3-Hydroxyisobutyrate	0.004±0.002	0.024±0.021	0.0435	1.000
3-Hydroxybutyrate	0.003±0.002	0.012±0.012	0.0881	0.847
Alanine	0.015±0.003	0.038±0.023	0.0364	0.833
Glycine	0.057±0.005	0.055±0.085	0.9432	0.833
Methionine	0.056±0.003	0.025±0.027	0.0208	0.833
Tyrosine	0.049±0.006	0.023±0.026	0.0324	0.833
Glutamate	0.066±0.002	0.052±0.083	0.6943	0.833
Acetate	0.005±0.002	0.023±0.019	0.0356	0.792
Leucine	0.111±0.160	0.050±0.083	0.4581	0.778
Valine	0.029±0.010	0.015±0.018	0.1174	0.750
Ascorbate	0.054±0.026	0.030±0.040	0.2642	0.750
Isoleucine	0.037±0.003	0.025±0.031	0.3516	0.694
Fumarate	0.060±0.004	0.039±0.028	0.1026	0.667
Glutamine	0.065±0.004	0.118±0.145	0.3916	0.667
Phenylalanine	0.052±0.005	0.063±0.072	0.7151	0.639
Methylmalonate	0.031±0.006	0.051±0.066	0.4902	0.611
Creatine	0.008±0.005	0.030±0.047	0.2904	0.583
Citrate	0.004±0.002	0.005±0.005	0.6046	0.556
Histidine	0.041±0.005	0.111±0.138	0.2444	0.500
Taurine	0.054±0.005	0.101±0.103	0.2913	0.500
Glucose	0.050±0.006	0.290±0.545	0.3060	0.500

Table 4.3.3: Area under the curve of metabolites detected in the blood plasma from fibrotic livers.

	CCl_4-induced fibrosis (Septal fibrosis)	ALK5 targeting (Biliary fibrosis)
3-Hydroxybutyrate	ND	0.847
3-Hydroxyisobutyrate	ND	1.000
Acetate	1.000	0.792
Alanine	0.815	0.833
Ascorbate	ND	0.750
Betaine	0.963	ND
Citrate	0.962	0.556
Creatine	0.741	0.583
Ethanol	1.000	ND
Formate	0.667	1.000
Fumarate	ND	0.667
Glucose	1.000	0.500
Glutamate	ND	0.833
Glutamine	0.926	0.667
Glycine	ND	0.833
Histidine	ND	0.500
Isoleucine	ND	0.694
Lactate	1.000	1.000
Leucine	ND	0.778
Methionine	ND	0.833
Methylmalonate	ND	0.611
O-phosphocholine	0.741	ND
Phenylalanine	0.963	0.639
Pyruvate	0.796	ND
Taurine	ND	0.500
Tyrosine	0.519	0.833
Valine	0.667	0.750

ND: Not-Detected.

DISCUSSION

The metabolic status of the liver is mainly investigated by transcriptomics, proteomics and epigenomics (Markley et al., 2017; Nwosu et al., 2017) and depends on structural alterations (Hammad et al., 2017). Therefore, metabolic profiling provides an accurate dimension for the physiological and pathological state of the liver (Markley et al., 2017). Based on the metabolic status of hepatocytes (Colnot and Perret, 2011; Ghafoory et al., 2013; Majumdar and Pinzani, 2016) the liver is divided into three zones: i) Zone I (Periportal) receives high levels of oxygen and blood rich in nutrients; ii) Zone III (Pericentral) has low levels of oxygen and blood poor in nutrients; and iii) Zone II (Midzonal) lies in between the two previous zones. Hence, any perturbation of a specific metabolic zone is directly reflected in metabolite levels. Beside this, several attempts to establish metabolite-based biomarkers for liver diseases in rodents (Gou et al., 2013; Wang et al., 2016) and humans (Gao et al., 2015; Emwas et al., 2016; Shariff et al., 2017) have recently been reported. Therefore, I am trying to use a cutting-edge technology (NMR-based metabolic profiling) to identify biomarkers for liver disease staging in a minimal-invasive way. In addition, these unfocused metabolomics in blood plasma and liver tissue helps hepatologists and provides one layer - functional in vivo assay- for systems biologists.

NMR-based metabolic profiling of biological fluids and solid tissues is chosen in this study for several reasons: i) Neither extensive sample preparation nor derivatization is required, which in most cases leads to false positive or negative results; ii) Destructive preparation is minimal and sample recovery is possible; iii) Quantitative analysis of all detectable metabolites from very tiny specimens (0.15-0.75mg of solid tissue and ~100µl of blood plasma) is possible; and iv) Elucidation of the dynamicity and the compartmentalization of metabolic pathways. Beside others, these advantages of NMR-based metabolomics were recently reviewed by Amathieu et al., (2016) as well as by Markley and colleagues (2017). Several hundred reports have also attempted to use NMR technology for metabolic profiling of urine, plasma, serum and tissue extracts (Beckonert et al., 2007; Teahan et al., 2007; Bouatra et al., 2013; Dona et al., 2014; Gogiashvili et al., 2017).

CHAPTER 5: DISCUSSION

Carbon tetrachloride (CCl_4) is a well-accepted model for liver intoxication, regeneration and fibrosis studies in rodents. Briefly, injection of a single toxic dose of CCl_4 is inducing a highly reproducible necro-inflammatory process followed by regenerative events (Hoehme et al., 2010; Zellmer et al., 2010; Hammad et al., 2014). However, administration of repeated doses of CCl_4 gives rise to the deposition of extracellular matrix in the pericentral (zone III) areas (septal) and to the neighboring ones (Krizhanovsky et al., 2008; Ding et al., 2014; Nussler et al., 2014; Hammad et al., 2017). Therefore, this acute and chronic mouse intoxication is an optimal model for pericentral (centrilobular) hepatocyte injury. In this study, I applied both acute and chronic CCl_4 models and followed up the metabolite alterations. Moreover, biliary type (Zone I) fibrosis induced by ABCB4 (MDR2) deletion and an attempt to normalize liver disease by ALK5 inhibitor was analyzed. These aforementioned rodent models represent the majority of liver fibrosis reported in clinical settings.

Clinically, the diagnosis of liver diseases is based on clinical parameters e.g. of ALT and AST as well as on invasive biopsy analysis. However, careful inspection reveals the main problems of these blood based parameters, i.e. i) Sensitivity: Most of these parameters are not liver specific, as e.g. AST is also found in skeletal muscles, kidney and brain; ii) These parameters are not changed during disease progression; and iii) These parameters are not able to detect early stages of liver disease. These pitfalls can be demonstrated using AUC curves for septal versus biliary fibrosis data as obtained in this study (Table 5.1). In septal fibrosis (induced by repeated administration of CCl_4), the levels of liver enzymes, namely of ALT, AST and AAR, are not sensitive to disease progression as the AUC values are 1.000 after 2, 4 and 6 weeks throughout. However, in biliary fibrosis (genetically-induced fibrosis and targeted by Ly2152799), these enzymes are not able to optimally predict the disease as AUC values are as low as 0.669, 0.667 and 0.567 after 2, 4 and 6 weeks, respectively.

Table 5.1. Area under the curve of metabolites detected in the blood plasma from mice with fibrotic livers to identify disease as well as progression associated markers.

	Parameters	CCl_4-induced fibrosis (Septal fibrosis)			ALK5 targeting (Biliary fibrosis)
		2W vs 0W	4W vs 0W	6W vs 0W	Ly vs Veh
Liver transaminases	ALT	1.000	1.000	1.000	0.694
	AST	1.000	1.000	1.000	0.667
	AAR	1.000	0.778	0.778	0.567
Tissue based	α-SMA	1.000	1.000	1.000	ND
	PSR	1.000	1.000	1.000	0.861
Blood plasma metabolic profiling	3-Hydroxybutyrate	ND	ND	ND	0.847
	3-Hydroxyisobutyrate	ND	ND	ND	1.000
	Acetate	1.000	1.000	1.000	0.792
	Alanine	0.667	0.889	0.889	0.833
	Ascorbate	ND	ND	ND	0.750
	Betaine	1.000	0.889	1.000	ND
	Citrate	0.778	1.000	1.000	0.556
	Creatinine	0.667	0.778	0.778	0.583
	Ethanol	1.000	1.000	1.000	ND
	Formate	0.667	0.667	0.667	1.000
	Fumarate	ND	ND	ND	0.667
	Glucose	1.000	1.000	1.000	0.500
	Glutamate	ND	ND	ND	0.833
	Glutamine	0.889	0.889	1.000	0.667
	Glycine	ND	ND	ND	0.833
	Histidine	ND	ND	ND	0.500
	Isoleucine	ND	ND	ND	0.694
	Lactate	1.000	1.000	1.000	1.000
	Leucine	ND	ND	ND	0.778
	Methionine	ND	ND	ND	0.833
	Methylmalonate	ND	ND	ND	0.611
	O-phosphocholine	0.778	0.667	0.778	ND
	Phenylalanine	1.000	0.889	1.000	0.639
	Pyruvate	0.556	1.000	0.833	ND
	Taurine	ND	ND	ND	0.500
	Tyrosine	0.667	0.778	0.556	0.833
	Valine	0.667	0.667	0.667	0.750

ND: Not detected.

Therefore, finding liver specific, blood-based and disease associated marker(s) is of high clinical importance. Lactate represents one of major altered metabolites in both models and is associated with liver diseases. The area under the curve of lactate is 1.00 (Table 5.1.) indicating that it is an optimal liver disease predictor but not well suited to predict disease progression. In agreement with these findings, it has been previously described that under different liver disease settings e.g. acute liver failure (Jeppesen et al., 2013) and hepatocellular carcinoma (Teilhet et al., 2017) lactate is released by accelerated splanchnic glycolysis and reduced hepatic gluconeogenesis. Moreover, the interplay between liver and muscles clearly shows that muscle lactate is metabolized to glucose in the liver (Cori cycle or lactic acid cycle). Regardless of the spatial distribution of extracellular matrix, blood plasma lactate is therefore elevated, proving its clinical relevance as a prognostic marker after validation in patient cohorts as well as for mechanistically-oriented studies as a functional assay.

The second consistently altered circulating metabolite is alanine, where in both models AUC is 0.8 (Table 4.3.2) in agreement with two reports (Johnston and Alberti, 1976; Gao et al., 2015) dealing with hepatitis and hepatocellular carcinoma patients. On one hand this indicates that alanine can predict liver damage development and progression as well as it is positively (not significantly) correlated with transaminases and PSR (Figure 4.6). On the other hand, understanding the complexity of the alanine cycle or the glucose-alanine cycle is of basic research value. Similarly to the Cori cycle, it is generally accepted that alanine is metabolized to glucose in the liver and vice versa in the skeletal muscle including pyruvate as an intermediate product (Figure 5.1). Thus, the circulating lactate, alanine and glucose levels are of clinical and functional value. Moreover, it is worth to mention that the plasma levels of both metabolites are negatively correlated with tissue levels indicating a metabolic deficit in the liver. This deficit leads to the accumulation of these metabolites in the blood. By careful analysis of the level of the intermediate –pyruvate- we found that it is also accumulated in the blood and the AUC value in case of septal fibrosis is 0.796 (Table 4.3.2). Furthermore, the pyruvate level in the blood is significantly correlated with alanine and positively (not significantly) correlated with standard fibrosis indices.

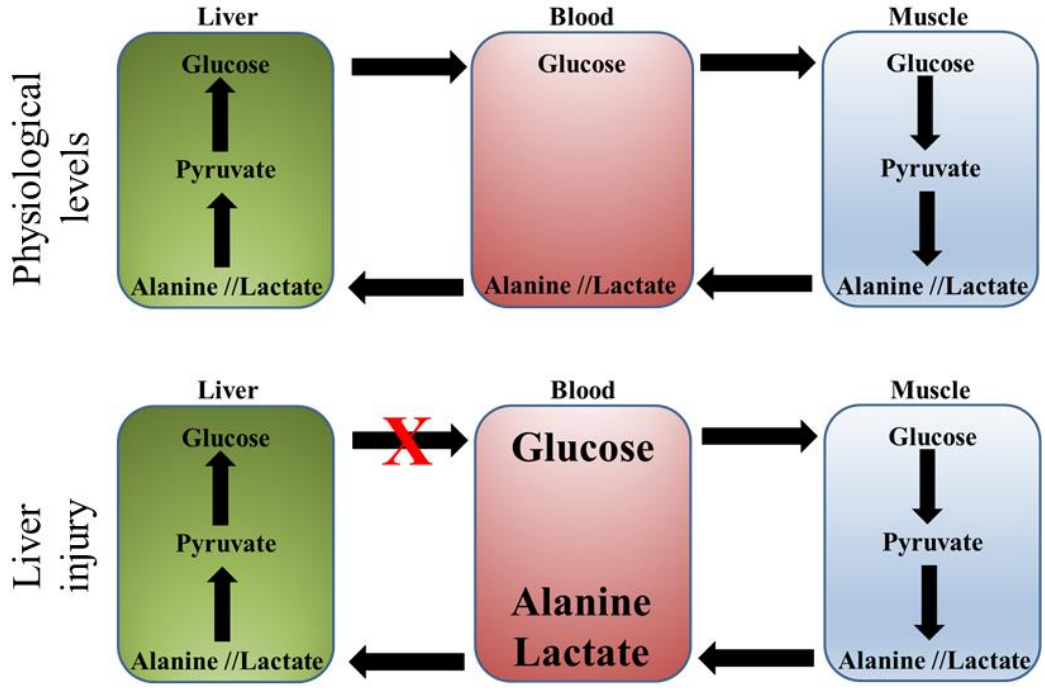

Figure 5.1: The interplay between liver and muscles for lactate, alanine and glucose levels to reach organism homeostasis.

It is known that patients with acute fulminant liver failure have high plasma glutamine levels (Harada et al., 2016; Helling et al., 2016). Most likely, this level is related to high ammonia and associated with hepatic encephalopathy. Under physiological conditions, glutamine is synthetized in the pericentral compartment (catalysed by glutamine synthetase) and is consumed with ammonia in the periportal hepatocytes to form glutamate. The latter reaction is catalysed by glutaminase and considered one pathway to detoxify ammonia (Ghafoory et al., 2013). Therefore, as the mechanism of consuming ammonia, glutamine and glutamate is inefficient in the case of liver diseases, their levels are increased in the blood plasma. We record that the AUC values of glutamine are 0.926 and 0.667 for septal and biliary fibrosis, respectively. Understanding this crosstalk between glutamine and glutamate and extrahepatic contributions is of relevance for functional aspects of ammonia detoxification and the urea cycle.

Furthermore, the phenylalanine metabolism to tyrosine via hydroxylation is considered the main source of tyrosine in the blood (Tessari et al., 2010). Surprisingly, the phenylalanine

level is well-correlated with liver disease progression, where the AUC values are 1.00, 0.89 and 1.00 after 2, 4 and 6 weeks, respectively, indicating that this metabolite might be a good progression-associated marker. This is in good agreement with a previous report on advanced fibrosis (Embade et al., 2016) and hepatocellular carcinoma (Gao et al., 2015). However, in biliary fibrosis, phenylalanine is not improving the disease predictability compared to liver transaminases. In contrast, tyrosine is well correlated, better than transaminases, with biliary fibrosis prediction.

To conclude, careful analysis of metabolic profiling revealed that there are some metabolites detected only in case of septal fibrosis including betaine, ethanol, o-phosphocholine and pyruvate. Among those metabolites, the betaine, o-phosphocholine and pyruvate levels are well-associated with disease progression. Betaine is one of the choline metabolites. It was shown that the blood betaine is significantly increased in liver diseases due to inhibition of choline degradation (Bollard et al., 2010). Surprisingly, the ethanol level is increased after CCl_4 intoxication and is mediated by decreasing the activities of the liver enzymes alcohol dehydrogenase isoenzymes and aldehyde dehydrogenase (Pron'ko et al., 2002). I could not detect ethanol in blood from biliary fibrosis and this supports the previous explanation. However, numerous metabolites are detected in case of biliary fibrosis, namely 3-hydroxybutyrate, 3-hydroxyisobutyrate, ascorbate, glycine, leucine, methionine and valine. These metabolites are good predictors for liver fibrosis as the AUC values are higher than those for the liver enzymes. Therefore, I can conclude that my study shed light on the usability of blood-based metabolites as i) Liver disease biomarkers; ii) Disease progression associated metabolites; and iii) Markers for metabolic zonation studies.

SUMMARY

Chronic liver disease is a common clinical problem. Currently, the diagnosis is based on non-invasive techniques like e.g. fibroscan, MRI, elastography, on minimal-invasive techniques like e.g. liver transaminases, and on the invasive biopsy method. However, these aforementioned methods have several drawbacks. Briefly, non-invasive methods are usually not-sensitive to early chronic liver disease; whereas blood based liver enzymes are not specific for liver. Therefore, the gold standard for the diagnosis of hepatic diseases is the histological assessment of liver biopsies. The use of liver biopsies is, however, subject to sampling- as well as inter- and intra-observer variability. These limitations affect the diagnostic accuracy, reliability, and responsiveness of treatment end-points. Moreover, liver biopsies are risky for the patient because of potential bleeding, organ perforation and even death. Thus, an urgent medical need exists for reliable and highly accurate treatment end-point indicators that can replace liver biopsies.

In this thesis the use of metabolite screening for diagnosis and staging is suggested to be used. It is well accepted that acute and chronic intoxications alter the regulation of liver metabolism at different levels. The blood or urine metabolome should therefore represent the final outcome of liver cellular regulation and the phenotype of a disease. The scope of this thesis is to establish and to validate marker(s) based on metabolite levels, both for the early diagnosis of liver diseases and for the prediction of liver disease progression. To achieve this goal, a metabolite screening for diagnosis and staging was performed to identify the presence and severity of inflammation and fibrosis in murine livers and blood. To characterize the metabolic alterations upon acute and chronic liver intoxications, nuclear magnetic resonance (NMR) spectroscopy was employed. NMR is fully quantitative, highly reproducible, detects all metabolites simultaneously in one non selective measurment, it is non-invasive, non-destructive and allows for a complete recovery of the sample. Moreover, just a minimum of sample preparation with no need for derivatization is required.

CHAPTER 6: SUMMARY

In order to induce acute toxic liver injuries, male C57BL/6N mice exposed to a single dose of CCl_4 were used. Moreover, chronic liver damage was induced by repeated injections of CCl_4 for 6 weeks. At specific time points both blood and livers of the mice were harvested. A control group received the same dose of just olive oil. Three to four mice were used for each group. Further, MDR2-/- mice (6 months old) were treated with Ly2157299 (Galunisertib; ALK5 inhibitor). ALK5 (TGFβ type I receptor kinase) was used to interfere with TGFβ signalling in MDR2-/- mice. Two groups of mice were used. Ly2157299 treated mice for 14 consecutive days (150 mg/kg) orally. The vehicle treated group received the same amount for 14 days orally. Two days after the last injection, both blood and livers were harvested.

Biochemical parameters e.g. ALT and AST increased during disease progression upon CCl_4 injection. This alteration was correlated with accumulation of extracellular matrix (ECM) and ECM-producing cells as indicated by picro-sirius red and alpha-SMA staining, respectively. These data give us a deep insight into the test models, where both acute and chronic liver damage were confirmed.

Blood plasma-based metabolic profiling was performed. Surprisingly, some metabolites e.g. acetate, alanine, formate, glucose, glutamine, lactate and phenylalanine are considered very good predictors for chronic liver diseases - regardless to spatial (septal or biliary fibrosis) extracellular matrix- as indicated by AUC approximately 1.000. However, in the septal CCl_4-induced fibrosis model betaine, citrate, glutamine and phenylalanine, however, in biliary fibrosis 3-Hydroxyisobutyrate, formate, glutamate, glycine, methionine and tyrosine can be used to stage the disease. These differences in metabolite levels can be explained by hepatic zonation of extracellular matrix deposition. It is generally accepted that in CCl_4 induced injury, glutamine synthesis, glycolysis, tricarboxylic acid cycle and phase I as well as phase II drug metabolism are principally altered. Whereas urea formation, gluconeogenesis and oxidative phosphorylation are mainly affected in case of biliary

fibrosis, further validation in clinical cohorts is absolutely mandatory and will be a follow-up story.

My study shed light on the importance of the metabolites identified in septal and biliary fibrosis: i) Validation in clinical cohorts of circulatory based liver disorders (septal fibrosis) and cholestasis (biliary fibrosis); this provides the scientists working in the field of liver diseases with a list of biomarkers; ii) Molecular analysis of chronic liver disease progression and comparing this blood based metabolic profiling with liver tissue to mechanistically understand disease dynamics; and iii) Providing metabolism scientists with quantitative data for single metabolites in a time-dependent manner for further functional analysis.

ZUSAMMENFASSUNG

Identifizierung von metabolischen Prognosemarkern bei Lebererkrankungen nach Tetrachlorkohlenstoff intoxikation

Chronische Lebererkrankungen sind ein häufiges klinisches Problem. Gegenwärtig basiert die Diagnose auf nicht-invasiven Verfahren wie z.B. Fibroscan, MRT und Elastographie, sowie auf minimal-invasiven Verfahren wie z.B. Bestimmungen der Lebertransaminasen und schließlich auf der invasiven Biopsie-Methode. Die genannten Verfahren haben jedoch einige Nachteile. So sind nicht-invasive Verfahren in der Regel nicht zur Früherkennung von chronischen Lebererkrankungen geeignet, während die Leberenzyme im Blut keine für die Leber spezifischen Aussagen erlauben. Der Gold-Standard für die Diagnose von Lebererkrankungen ist daher die histologische Beurteilung von Leberbiopsien. Die Verwendung von Leberbiopsien unterliegt jedoch Unsicherheiten sowohl bei der Probennahme als auch durch Inter- und Intrabeobachter-Variabilität. Diese Einschränkungen beeinflussen die diagnostische Genauigkeit, die Zuverlässigkeit und das Ansprechen der Methode auf den Behandlungserfolg. Darüber hinaus sind Leberbiopsien für den Patienten wegen möglicher Blutungen, Organperforation und einer nicht zu vernachlässigenden Letalitätsquote riskant. Daher besteht ein dringender medizinischer Bedarf an zuverlässigen und hochgenauen Behandlungsendpunkt-Indikatoren, die Leberbiopsien ersetzen können.

In dieser Arbeit wird die Verwendung eines Metabolit-Screenings für die Diagnose und die Beurteilung des Verlaufs von Lebererkrankungen vorgeschlagen. Es ist allgemein anerkannt, dass akute und chronische Leberschädigungen die Regulation des Lebermetabolismus auf verschiedenen Ebenen verändern. Das Blut- oder Urin-Metabolom sollte daher das endgültige Ergebnis der Leberzellregulation und des Phänotyps einer Krankheit wiedergeben. Der Gegenstand dieser Arbeit ist die Etablierung und Validierung von Markern basierend auf Metabolitenkonzentrationen, sowohl für die Früherkennung von Lebererkrankungen als auch für die Vorhersage des Verlaufs der Lebererkrankung. Dazu wurde ein Metabolit-Screening für die Diagnose und die Untersuchung des

Krankheitsverlaufs durchgeführt, um das Vorhandensein und die Schwere von der Entzündung und der Fibrose in den Lebern und im Blut von Mäusen nachzuweisen. Zur Charakterisierung der metabolischen Veränderungen bei akuten und chronischen Leberschädigungen wurde die kernmagnetische Resonanzspektroskopie (NMR-Spektroskopie) eingesetzt. Die NMR ist vollständig quantitativ, gut reproduzierbar, detektiert alle Metaboliten gleichzeitig in einer nichtselektiven Messung, ist nicht-invasiv, zerstörungsfrei und ermöglicht eine vollständige Rückgewinnung der Probe. Darüber hinaus ist nur ein Minimum an Probenvorbereitung ohne die Notwendigkeit einer Derivatisierung der Probe erforderlich. Um akute toxische Leberschädigungen zu induzieren, wurden männliche C57BL / 6N-Mäuse, die eine einzige CCl_4-Injektion erhalten haben, verwendet. Darüber hinaus wurde eine chronische Leberschädigung durch wiederholte Injektionen von CCl_4 über 6 Wochen induziert. Zu bestimmten Zeitpunkten wurden sowohl das Blut als auch die Lebern der Mäuse entnommen. Eine Kontrollgruppe erhielt die gleiche Dosis an reinem Olivenöl. Drei bis vier Mäuse wurden für jede Gruppe verwendet. Weiterhin wurden MDR2 -/- Mäuse (4 Monate alt) mit Ly2157299 (Galunisertib; ALK5-Inhibitor) behandelt. ALK5 (TGFβ Typ I Rezeptorkinase) wurde verwendet, um das TGFβ-Signalling in MDR2 -/- Mäusen zu stören. Zwei Gruppen von Mäusen wurden verwendet: Ly2157299 wurde an die behandelten Mäuse für 14 aufeinanderfolgende Tage (150 mg / kg) oral verabreicht. Die Kontrollgruppe erhielt die gleiche Menge an Olivenöl für 14 Tage oral. Zwei Tage nach der letzten Injektion wurden sowohl Blut als auch Lebern entnommen.

Biochemische Parameter, z.B. ALT und AST, nahmen während des Verlaufs der Erkrankung nach einer CCl_4-Injektion zu. Diese Veränderungen waren mit der Anhäufung von extrazellulärer Matrix (ECM) und ECM-produzierenden Zellen korrelierbar, wie durch Picro-Sirius-Rot- bzw. Alpha-SMA-Färbung gezeigt werden konnte. Diese Daten geben uns einen tiefen Einblick in die Testmodelle, bei denen sowohl akute als auch chronische Leberschäden bestätigt werden konnten. Auch für das Blutplasma der Mäuse wurde ein metabolisches Profil erstellt. Überraschenderweise deuten AUC-Werte von nahe 1.000 für

einige Metabolite, z.B. für Acetat, Alanin, Formiat, Glukose, Glutamin, Laktat und Phenylalanin an, dass sie als sehr gute Indikatoren für chronische Lebererkrankungen betrachtet werden können, unabhängig von der räumlichen extrazellulären Matrix (Septum- oder Gallenfibrose). Im Modell der CCl_4-induzierten Septumfibrose können Betain, Citrat, Glutamin und Phenylalanin für das die Untersuchung des Krankheitsverkaufs verwendet werden, während dazu bei der Gallenfibrose 3-Hydroxyisobutyrat, Formiat, Glutamat, Glycin, Methionin und Tyrosin verwendet werden müssen. Diese Unterschiede in den Metabolitenkonzentrationen können durch hepatische Zonierung der extrazellulären Matrixdeposition erklärt werden. Es ist allgemein akzeptiert, dass bei einer CCl_4-induzierten Leberschädigung die Glutaminsynthese, die Glykolyse, der Tricarbonsäurezyklus sowie der Arzneimittelmetabolismus der Phase I und der Phase II prinzipiell gestört sind. Bei der Gallenfibrose sind jedoch hauptsächlich Harnstoffbildung, Glukoneogenese und oxidative Phosphorylierung betroffen. Eine weitere Validierung in klinischen Kohorten ist zwingend erforderlich und wird als Follow-Up-Studie durchgeführt.

Unsere Studie beleuchtet die Bedeutung der identifizierten Metaboliten bei Septum- und Gallenfibrose: i) Validierung der Kreislauf-basierten Leberfunktionsstörungen (Septumfibrose) und der Cholestase (Gallenfibrose) in klinischen Kohorten; die Ergebnisse liefern Wissenschaftlern, die an der Untersuchung von Lebererkrankungen arbeiten, eine Liste von Biomarkern; ii) Molekulare Analyse des Verlaufs der chronischen Lebererkrankung und Vergleich der metabolischen Profile von Blutplasma und Lebergewebe, um die Krankheitsdynamik mechanistisch zu verstehen; und iii) Bereitstellung von quantitativen, zeitabhängigen Daten für einzelne Metabolite für die weitere funktionelle Analyse durch Systembiologen.

ABSTRACT

Currently, the golden standards of liver disease diagnosis are based on histological assessments of biopsies and some clinical parameters. The use of liver biopsies, however, is not without cost or risk (bleeding, perforation, death). Furthermore, liver biopsies can be subjected to sampling and inter- and intra-observer variabilities. Moreover, most of clinical parameters are not liver specific and might not be sensitive to predict minimal alterations and disease progression. Therefore, we aim to identify minimal invasive biomarker(s) that can be used to differentiate stages of liver disease. Metabolomics profiling of healthy and CCl_4-induced fibrotic mice using an updated version of Nuclear Magnetic Resonance (MAS-^{1}H-NMR) was performed. We have investigated the fingerprints of fibrosis progression by biochemical, histopathological, and metabolomics as well as gene expression analysis in a time-resolved experiment in both models. Biochemical parameters like e.g. ALT and AST were increased during disease progression upon CCl_4 injection. This alteration was correlated with the accumulation of extracellular matrix (ECM) as indicated by picro-sirius red and hematoxylin and eosin staining. Furthermore, blood plasma-based metabolic profiling revealed that several metabolites namely, acetate, ethanol, glucose and lactate significantly reflect the disease as indicated by AUC values (1.00) compared to healthy mice. Some metabolites e.g. betaine, phenylalanine, citrate, glutamine, alanine, pyruvate, creatinine and O-phosphocholine could also be used to predict the disease stages, however, the AUC values was in the range between 0.74 and 0.963 and differed according to the disease stage. Formate, valine and tyrosine were shown to be identified as poorly predictors where the AUC values of which were in a range between 0.52 and 0.67. A further clinical validation of the very good predictors is ongoing.

REFERENCES

- Alam TM, Jenkins JE (2012) Advanced Aspects of Spectroscopy, book edited by Muhammad Akhyar Farrukh, Chapter 10: HR-MAS NMR Spectroscopy in Material Science:279-306.

- Amathieu R, Nahon P, Triba M, Bouchemal N, Trinchet JC, Beaugrand M, Dhonneur G, Le Moyec L. Metabolomic approach by 1H NMR spectroscopy of serum for the assessment of chronic liver failure in patients with cirrhosis. J Proteome Res. 2011 Jul 1;10(7):3239-45.

- Amathieu R, Triba MN, Goossens C, Bouchemal N, Nahon P, Savarin P, Le Moyec L. Nuclear magnetic resonance based metabolomics and liver diseases: Recent advances and future clinical applications. World J Gastroenterol. 2016 Jan 7;22(1):417-26. Review.

- Bacon BR, O'Grady JG, Di Bisceglie AM and Lake JR (2006) Comprehensive clinical hepatology. Mosby publisher, second edition, printed in China.

- Baniasadi H, Gowda GA, Gu H, Zeng A, Zhuang S, Skill N, Maluccio M, Raftery D. Targeted metabolic profiling of hepatocellular carcinoma and hepatitis C using LC-MS/MS. Electrophoresis. 2013 Oct;34(19):2910-7.

- Barberá-Guillem E, Alonso-Varona A, Boyano MD, Vidal-Vanaclocha F. Estimating anatomical-functional position coordinates in liver tissue. Anat Rec. 1990 Nov;228(3):267-76.

- Bataller R, Brenner DA. Liver fibrosis. J Clin Invest. 2005 Feb;115(2):209-18. Review.

- Beckonert O, Keun HC, Ebbels TM, Bundy J, Holmes E, Lindon JC, Nicholson JK. Metabolic profiling, metabolomic and metabonomic procedures for NMR spectroscop y of urine, plasma, serum and tissue extracts. Nat Protoc. 2007;2(11):2692-703.

- Böhm F, Köhler UA, Speicher T, Werner S. Regulation of liver regeneration by growth factors and cytokines. EMBO Mol Med. 2010 Aug;2(8):294-305. Review.

- Bollard ME, Contel NR, Ebbels TM, Smith L, Beckonert O, Cantor GH, Lehman-McKeeman L, Holmes EC, Lindon JC, Nicholson JK, Keun HC. NMR-based metabolic profiling identifies biomarkers of liver regeneration following partial hepatectomy in the rat. J Proteome Res. 2010 Jan;9(1):59-69.

- Bouatra S, Aziat F, Mandal R, Guo AC, Wilson MR, Knox C, Bjorndahl TC, Krishnamurthy R, Saleem F, Liu P, Dame ZT, Poelzer J, Huynh J, Yallou FS, Psychogios N, Dong E, Bogumil R, Roehring C, Wishart DS. The human urine metabolome. PLoS One. 2013 Sep 4;8(9):e73076.

- Boyer TD, Wright TL and Manns MP (2006) Zakim and Boyer's hepatology: A textbook of liver disease. Saunders, Elsevier Inc, volume 1, fifth edition, printed in Canada.

- Braeuning A, Singh Y, Rignall B, Buchmann A, Hammad S, Othman A, von Recklinghausen I, Godoy P, Hoehme S, Drasdo D, Hengstler JG, Schwarz M. Phenotype and growth behavior of residual β-catenin-positive hepatocytes in livers of β-catenin-deficient mice. Histochem Cell Biol. 2010 Nov;134(5):469-81.

- Clayton TA, Baker D, Lindon JC, Everett JR, Nicholson JK. Pharmacometabonomic identification of a significant host-microbiome metabolic interaction affecting human drug metabolism. Proc Natl Acad Sci U S A. 2009 Aug 25;106(34):14728-33.

- Colnot S, Perret C (2011) Liver Zonation. In: Monga S. (eds) Molecular Pathology of Liver Diseases. Molecular Pathology Library, vol 5. Springer, Boston, MA.

- Diaz Gómez MI, Fanelli SL, Delgado de Layño AM, Castro JA, Castro GD. Liver nuclear and microsomal CYP2E1-mediated metabolism of xenobiotics in rats

chronically drinking an alcohol-containing liquid diet. Toxicol Ind Health. 2006 Oct;22(9):367-74.

- Ding BS, Cao Z, Lis R, Nolan DJ, Guo P, Simons M, Penfold ME, Shido K, Rabbany SY, Rafii S. Divergent angiocrine signals from vascular niche balance liver regeneration and fibrosis. Nature. 2014 Jan 2;505(7481):97-102.

- Dituri F, Mazzocca A, Fernando J, Papappicco P, Fabregat I, De Santis F, Paradiso A, Sabbà C, Giannelli G. Differential Inhibition of the TGF-β Signaling Pathway in HCC Cells Using the Small Molecule Inhibitor LY2157299 and the D10 Monoclonal Antibody against TGF-β Receptor Type II. PLoS One. 2013 Jun 27;8(6):e67109.

- Domenicali M, Caraceni P, Giannone F, Baldassarre M, Lucchetti G, Quarta C, Patti C, Catani L, Nanni C, Lemoli RM, Bernardi M. A novel model of CCl4-induced cirrhosis with ascites in the mouse. J Hepatol. 2009 Dec;51(6):991-9.

- Dona AC, Jiménez B, Schäfer H, Humpfer E, Spraul M, Lewis MR, Pearce JT, Holmes E, Lindon JC, Nicholson JK. Precision high-throughput proton NMR spectroscopy of human urine, serum, and plasma for large-scale metabolic phenotyping. Anal Chem. 2014 Oct 7;86(19):9887-94.

- Embade N, Mariño Z, Diercks T, Cano A, Lens S, Cabrera D, Navasa M, Falcón-Pérez JM, Caballería J, Castro A, Bosch J, Mato JM, Millet O. Metabolic Characterization of Advanced Liver Fibrosis in HCV Patients as Studied by Serum 1H-NMR Spectroscopy. PLoS One. 2016 May 9;11(5):e0155094.

- Emwas AH, Roy R, McKay RT, Ryan D, Brennan L, Tenori L, Luchinat C, Gao X, Zeri AC, Gowda GA, Raftery D, Steinbeck C, Salek RM, Wishart DS. Recommendations and standardization of biomarker quantification using NMR-based metabolomics with particular focus on urine analysis. J Proteome Res. 2016 Feb 5;15(2):360-73.

- Friedman SL. Hepatic fibrosis -- overview. Toxicology. 2008 Dec 30;254(3):120-9.

- Gao R, Cheng J, Fan C, Shi X, Cao Y, Sun B, Ding H, Hu C, Dong F, Yan X. Serum Metabolomics to Identify the Liver Disease-Specific Biomarkers for the Progression of Hepatitis to Hepatocellular Carcinoma. Sci Rep. 2015 Dec 10;5:18175.

- Gebhardt R. Metabolic zonation of the liver: regulation and implications for liver function. Pharmacol Ther. 1992;53(3):275-354. Review.

- Geerts A. History, heterogeneity, developmental biology, and functions of quiescent hepatic stellate cells. Semin Liver Dis. 2001 Aug;21(3):311-35. Review.

- Ghafoory S, Breitkopf-Heinlein K, Li Q, Scholl C, Dooley S, Wölfl S. Zonation of nitrogen and glucose metabolism gene expression upon acute liver damage in mouse. PLoS One. 2013 Oct 17;8(10):e78262.

- Giannelli G, Mikulits W, Dooley S, Fabregat I, Moustakas A, ten Dijke P, Portincasa P, Winter P, Janssen R, Leporatti S, Herrera B, Sanchez A. The rationale for targeting TGF-β in chronic liver diseases. Eur J Clin Invest. 2016 Apr;46(4):349-61. Review.

- Giannelli G, Villa E, Lahn M. Transforming growth factor-β as a therapeutic target in hepatocellular carcinoma. Cancer Res. 2014 Apr 1;74(7):1890-4. Review.

- Godoy P, Hewitt NJ, Albrecht U, Andersen ME, Ansari N, Bhattacharya S, Bode JG, Bolleyn J, Borner C, Böttger J, Braeuning A, Budinsky RA, Burkhardt B, et al. Recent advances in 2D and 3D in vitro systems using primary hepatocytes, alternative hepatocyte sources and non-parenchymal liver cells and their use in investigating mechanisms of hepatotoxicity, cell signaling and ADME. Arch Toxicol. 2013 Aug;87(8):1315-530. Review.

- Gogiashvili M, Edlund K, Gianmoena K, Marchan R, Brik A, Andersson JT, Lambert J, Madjar K, Hellwig B, Rahnenführer J, Hengstler JG, Hergenröder R, Cadenas C. Metabolic profiling of ob/ob mouse fatty liver using HR-MAS 1H-NMR combined with

gene expression analysis reveals alterations in betaine metabolism and the transsulfuration pathway. Anal Bioanal Chem. 2017 Feb;409(6):1591-1606.

- Gou X, Tao Q, Feng Q, Peng J, Zhao Y, Dai J, Wang W, Zhang Y, Hu Y, Liu P. Urine metabolic profile changes of CCl4-liver fibrosis in rats and intervention effects of Yi GuanJian Decoction using metabonomic approach. BMC Complement Altern Med. 2013 Jun 3;13:123.

- Gumucio JJ, Miller DL. Zonal hepatic function: solute-hepatocyte interactions within the liver acinus. Prog Liver Dis. 1982;7:17-30. Review.

- Hammad S, Braeuning A, Meyer C, Mohamed FEZA, Hengstler JG, Dooley S. A frequent misinterpretation in current research on liver fibrosis: the vessel in the center of CCl4-induced pseudolobules is a portal vein. Arch Toxicol. 2017 Aug 19. [Epub ahead of print].

- Hammad S, Hoehme S, Friebel A, von Recklinghausen I, Othman A, Begher-Tibbe B, Reif R, Godoy P, Johann T, Vartak A, Golka K, Bucur PO, Vibert E, Marchan R, Christ B, Dooley S, Meyer C, Ilkavets I, Dahmen U, Dirsch O, Böttger J, Gebhardt R, Drasdo D, Hengstler JG. Protocols for staining of bile canalicular and sinusoidal networks of human, mouse and pig livers, three-dimensional reconstruction and quantification of tissue microarchitecture by image processing and analysis. Arch Toxicol. 2014 May;88(5):1161-83.

- Harada S, Takebayashi T, Kurihara A, Akiyama M, Suzuki A, Hatakeyama Y, Sugiyama D, Kuwabara K, Takeuchi A, Okamura T, Nishiwaki Y, Tanaka T, Hirayama A, Sugimoto M, Soga T, Tomita M. Metabolomic profiling reveals novel biomarkers of alcohol intake and alcohol-induced liver injury in community-dwelling men. Environ Health Prev Med. 2016 Jan;21(1):18-26.

- Helling G, Wahlin S, Smedberg M, Pettersson L, Tjäder I, Norberg Å, Rooyackers O, Wernerman J. Plasma glutamine concentrations in liver failure. PLoS One. 2016 Mar 3;11(3):e0150440.

- Herbertz S, Sawyer JS, Stauber AJ, Gueorguieva I, Driscoll KE, Estrem ST, Cleverly AL, Desaiah D, Guba SC, Benhadji KA, Slapak CA, Lahn MM. Clinical development of galunisertib (LY2157299 monohydrate), a small molecule inhibitor of transforming growth factor-beta signaling pathway. Drug Des Devel Ther. 2015 Aug 10;9:4479-99.

- Hijmans BS, Grefhorst A, Oosterveer MH, Groen AK. Zonation of glucose and fatty acid metabolism in the liver: mechanism and metabolic consequences. Biochimie. 2014 Jan;96:121-9. Review.

- Hoehme S, Brulport M, Bauer A, Bedawy E, Schormann W, Hermes M, Puppe V, Gebhardt R, Zellmer S, Schwarz M, Bockamp E, Timmel T, Hengstler JG, Drasdo D. Prediction and validation of cell alignment along microvessels as order principle to restore tissue architecture in liver regeneration. Proc Natl Acad Sci USA. 2010 Jun 8;107(23):10371-6.

- Höhme S, Hengstler JG, Brulport M, Schäfer M, Bauer A, Gebhardt R, Drasdo D. Mathematical modelling of liver regeneration after intoxication with CCl(4). Chem Biol Interact. 2007 May 20;168(1):74-93.

- Hollander CF, van Bezooijen CF, Solleveld HA. Anatomy, function and aging in the mouse liver. Arch Toxicol Suppl. 1987;10:244-50. Review.

- Jeppesen JB, Mortensen C, Bendtsen F, Møller S. Lactate metabolism in chronic liver disease. Scand J Clin Lab Invest. 2013;73(4):293-9.

- Johnston DG, Alberti KG. Carbohydrate metabolism in liver disease. Clin Endocrinol Metab. 1976 Nov;5(3):675-702. Review.

- Katz NR. Metabolic heterogeneity of hepatocytes across the liver acinus. J Nutr. 1992 Mar;122(3 Suppl):843-9. Review.

- Krishna M. Microscopic anatomy of the liver. Clin Liver Dis. 2013;2(S1):1-7. Review.

- Krizhanovsky V, Yon M, Dickins RA, Hearn S, Simon J, Miething C, Yee H, Zender L, Lowe SW. Senescence of activated stellate cells limits liver fibrosis. Cell. 2008 Aug 22;134(4):657-67.

- Magami Y, Azuma T, Inokuchi H, Kokuno S, Moriyasu F, Kawai K, Hattori T. Cell proliferation and renewal of normal hepatocytes and bile duct cells in adult mouse liver. Liver. 2002 Oct;22(5):419-25.

- Majumdar A, Pinzani M. The holy grail of a biomarker for "liver function". Clinical Liver Disease 2016, 7:135–138.

- Manibusan MK, Odin M, Eastmond DA. Postulated carbon tetrachloride mode of action: a review. J Environ Sci Health C Environ Carcinog Ecotoxicol Rev. 2007 Jul-Sep;25(3):185-209. Review.

- Markley JL, Brüschweiler R, Edison AS, Eghbalnia HR, Powers R, Raftery D, Wishart DS. The future of NMR-based metabolomics. Curr Opin Biotechnol. 2017 Feb;43:34-40.

- Martínez-Granados B, Monleón D, Martínez-Bisbal MC, Rodrigo JM, del Olmo J, Lluch P, Ferrández A, Martí-Bonmatí L, Celda B. Metabolite identification in human liver needle biopsies by high-resolution magic angle spinning 1H NMR spectroscopy. NMR Biomed. 2006 Feb;19(1):90-100.

- Martins PN, Theruvath TP, Neuhaus P. Rodent models of partial hepatectomies. Liver Int. 2008 Jan;28(1):3-11. Review.

- Michalopoulos GK, Khan Z. Liver regeneration, growth factors, and amphiregulin. Gastroenterology. 2005 Feb;128(2):503-6.

- Michalopoulos GK. Liver regeneration. J Cell Physiol. 2007 Nov;213(2):286-300. Review.

- Moorman AF, Vermeulen JL, Charles R, Lamers WH. Localization of ammonia-metabolizing enzymes in human liver: ontogenesis of heterogeneity. Hepatology. 1989 Mar;9(3):367-72.

- Nussler AK, Wildemann B, Freude T, Litzka C, Soldo P, Friess H, Hammad S, Hengstler JG, Braun KF, Trak-Smayra V, Godoy P, Ehnert S. Chronic CCl4 intoxication causes liver and bone damage similar to the human pathology of hepatic osteodystrophy: a mouse model to analyse the liver-bone axis. Arch Toxicol. 2014 Apr;88(4):997-1006.

- Nwosu ZC, Megger DA, Hammad S, Sitek B, Roessler S, Ebert MP, Meyer C, Dooley S. Identification of the Consistently Altered Metabolic Targets in Human Hepatocellular Carcinoma. Cell Mol Gastroenterol Hepatol. 2017 May 31;4(2):303-323.

- O'Grady JG, Alexander GJ, Hayllar KM, Williams R. Early indicators of prognosis in fulminant hepatic failure. Gastroenterology. 1989 Aug;97(2):439-45.

- Othman A, Meyer, Telfah A, Lambert J, Hergenröder R, Dooley S, Hammad S. Tamoxifen is critical as inducer of Cre activity in mouse models for hepatotoxicity studies. Z Gastroenterol 2016; 54(12): 1343-1404. Presented in the 33th GASL, January 20-21, 2017, Essen-Germany.

- Phys. Org. Animal, human health benefits anticipated from university's premier biomedical, November 12th, 2013

- Poyer JL, McCay PB, Lai EK, Janzen EG, Davis ER. Confirmation of assignment of the trichloromethyl radical spin adduct detected by spin trapping during 13C-carbon

tetrachloride metabolism in vitro and in vivo. Biochem Biophys Res Commun. 1980 Jun 30;94(4):1154-60.

- Pron'ko PS, Satanovskaia VI, Gorenshteĭn BI, Kuz'mich AB, Pyzhik TN. Effect of pyruvate, threonine, and phosphoethanolamine on acetaldehyde metabolism in rats with toxic liver injury]. Vopr Med Khim. 2002 May-Jun;48(3):278-85.

- Qi J, Lang W, Geisler JG, Wang P, Petrounia I, Mai S, Smith C, Askari H, Struble GT, Williams R, Bhanot S, Monia BP, Bayoumy S, Grant E, Caldwell GW, Todd MJ, Liang Y, Gaul MD, Demarest KT, Connelly MA. The use of stable isotope-labeled glycerol and oleic acid to differentiate the hepatic functions of DGAT1 and -2. J Lipid Res. 2012 Jun;53(6):1106-16.

- Rappaport AM (1973) The microcirculatory hepatic unit. Microvasc Res. 6(2):212-28.

- Raucy JL and Carpenter SJ (1993).The expression of xenobiotic- metabolizing cytochromes P450 in fetal tissues. Journal of pharmacology and toxicology methods, Volume 29(39, Pages, 121-128.

- Ricken T, Werner D, Holzhütter HG, König M, Dahmen U, Dirsch O. Modelling functionperfusion behavior in liver lobules including tissue, blood, glucose, lactate and glycogen by use of a coupled two-scale PDE-ODE approach. Biomech Model Mechanobiol. 2015 Jun;14(3):515-36.

- Sahu SC (2007) Hepatotoxicity: From genomics to in vitro and in vivo models. John Wiley & Sons Ltd, printed in England.

- Saxena V, Gupta A, Nagana Gowda GA, Saxena R, Yachha SK, Khetrapal CL. 1H NMR spectroscopy for the prediction of therapeutic outcome in patients with fulminant hepatic failure. NMR Biomed. 2006 Aug;19(5):521-6.

- Shah H, Hartman SP, Weinhouse S. Formation of carbonyl chloride in carbon tetrachloride metabolism by rat liver in vitro. Cancer Res. 1979 Oct;39(10):3942-7.

- Shariff MIF, Kim JU, Ladep NG, Gomaa AI, Crossey MME, Okeke E, Banwat E, Waked I, Cox IJ, Williams R, Holmes E, Taylor-Robinson SD. The plasma and serum metabotyping of hepatocellular carcinoma in a Nigerian and Egyptian cohort using proton Nuclear Magnetic Resonance Spectroscopy. J Clin Exp Hepatol. 2017 Jun;7(2):83-92.

- Shi J, Aisaki K, Ikawa Y, Wake K. Evidence of hepatocyte apoptosis in rat liver after the administration of carbon tetrachloride. Am J Pathol. 1998 Aug;153(2):515-25.

- Slater TF, Cheeseman KH, Ingold KU. Carbon tetrachloride toxicity as a model for studying free-radical mediated liver injury. Philos Trans R Soc Lond B Biol Sci. 1985 Dec 17;311(1152):633-45.

- Stanciu A, Cotuţiu C, Amălinei C. New data about ITO cells. Rev Med Chir Soc Med Nat Iasi. 2002 Apr-Jun;107(2):235-9. Review.

- Teahan O, Gamble S, Holmes E, Waxman J, Nicholson JK, Bevan C, Keun HC. Impact of analytical bias in metabonomic studies of human blood serum and plasma. Anal Chem. 2006 Jul 1;78(13):4307-18.

- Teilhet C, Morvan D, Joubert-Zakeyh J, Biesse AS, Pereira B, Massoulier S, Dechelotte P, Pezet D, Buc E, Lamblin G, Peoc'h M, Porcheron J, Vasson MP, Abergel A, Demidem A. Specificities of human hepatocellular carcinoma developed on non-alcoholic fatty liver disease in absence of cirrhosis revealed by tissue extracts ^{1}H-NMR spectroscopy. Metabolites. 2017 Sep 22;7(4). pii: E49.

- Tessari P, Vettore M, Millioni R, Puricelli L, Orlando R. Effect of liver cirrhosis on phenylalanine and tyrosine metabolism. Curr Opin Clin Nutr Metab Care. 2010 Jan;13(1):81-6. Review.

- Wang EY, Yeh SH, Tsai TF, Huang HP, Jeng YM, Lin WH, Chen WC, Yeh KH, Chen PJ, Chen DS. Depletion of β-catenin from mature hepatocytes of mice promotes

expansion of hepatic progenitor cells and tumor development. Proc Natl Acad Sci U S A. 2011 Nov 8;108(45):18384-9.

- Wang G, Li Z, Li H, Li L, Li J, Yu C. Metabolic profile changes of CCl4-liver fibrosis and inhibitory effects of Jiaqi Ganxian Granule. Molecules 2016, 21(6), 698.

- Weber LW, Boll M, Stampfl A. Hepatotoxicity and mechanism of action of haloalkanes: carbon tetrachloride as a toxicological model. Crit Rev Toxicol. 2003;33(2):105-36. Review.

- Winnike JH, Li Z, Wright FA, Macdonald JM, O'Connell TM, Watkins PB. Use of pharmaco-metabonomics for early prediction of acetaminophen-induced hepatotoxicity in humans. Clin Pharmacol Ther. 2010 Jul;88(1):45-51.

- Yamada Y, Fausto N. Deficient liver regeneration after carbon tetrachloride injury in mice lacking type 1 but not type 2 tumor necrosis factor receptor. Am J Pathol. 1998 Jun;152(6):1577-89.

- Zellmer S, Schmidt-Heck W, Godoy P, Weng H, Meyer C, Lehmann T, Sparna T, Schormann W, Hammad S, Kreutz C, Timmer J, von Weizsäcker F, Thürmann PA, Merfort I, Guthke R, Dooley S, Hengstler JG, Gebhardt R. Transcription factors ETF, E2F, and SP-1 are involved in cytokine-independent proliferation of murine hepatocytes. Hepatology. 2010 Dec;52(6):2127-36.

- Zhang S, Sun WY, Wu JJ, Wei W. TGF-β signaling pathway as a pharmacological target in liver diseases. Pharmacol Res. 2014 Jul;85:15-22.

LIST OF PUBLICATIONS

- Bucur PO, Bekheit M, Audebert C, **Othman A,** Hammad S, et al. Modulating portal hemodynamics with vascular ring allows efficient regeneration after partial hepatectomy in a porcine model. **Ann Surg.** 2017 Feb 1. [Epub ahead of print]

- Bekheit M, Bucur PO, Audebert C, **Othman A,** Hammad S, et al., New technique for portal flow modulation in porcine major liver resection. **Clinics in Surgery** Dec 2016 1:1-2.
- Hammad S, Hoehme S, Friebel A, von Recklinghausen I, **Othman A,** Begher-Tibbe B, et al. Protocols for staining of bile canalicular and sinusoidal networks of human, mouse and pig livers, three-dimensional reconstruction and quantification of tissue microarchitecture by image processing and analysis. **Arch Toxicol.** 2014 May;88(5):1161-83.

- Lohr M, Edlund K, Botling J, Hammad S, Hellwig B, **Othman A,** Berglund A, et al. The prognostic relevance of tumour-infiltrating plasma cells and immunoglobulin kappa C indicates an important role of the humoral immune response in non-small cell lung cancer**. Cancer Lett.** 2013 Jun 10;333(2):222-8.

- Schmidt M, Hellwig B, Hammad S, **Othman A,** Lohr M, et al. A comprehensive analysis of human gene expression profiles identifies stromal immunoglobulin κ C as a compatible prognostic marker in human solid tumors. **Clin Cancer Res.** 2012 May 1;18(9):2695-703.
- Braeuning A, Singh Y, Rignall B, Buchmann A, Hammad S, **Othman A,** von Recklinghausen I, et al. Phenotype and growth behavior of residual β-catenin-positive hepatocytes in livers of β-catenin-deficient mice. **Histochem Cell Biol.** 2010 Nov;134(5):469-81.

MANUSCRIPT IN SUBMISSION

- Hammad S[1,2,*,#], **Othman A**[3,#], et al., Confounding influence of tamoxifen in mouse models of Cre recombinase-induced gene activation or inactivation (Archives of Toxicology 2018; In Revision). #equally contributed.

LIST OF PUBLICATIONS

ABSTRACTS/POSTERS

1. Othman A, et al. Identification of metabolic prognostic biomarkers in carbon tetrachloride induced liver fibrosis by using MAS-H1-NMR. Accepted as a poster in GASL **2018**, Hamburg-Germany.
2. Othman A, et al. Tamoxifen is critical as inducer of Cre activity in mouse models for hepatotoxicity studies. The 33th GASL, January 20-21, **2017**, Essen-Germany.
3. Hammad S, Telfah A, Othman A, et al. Systems analysis of the structural and molecular changes along the dynamics of liver fibrosis development. The 6th conference on Systems Biology of Mammalian Cells (SBMC), April 6-8, **2016**, Munic-Germany.
4. Celliere G, Boissier N, Othman A, et al. Towards improving in vitro–in vivo toxicity extrapolation using multi-scale modeling: A proof of concept on paracetamol hepatotoxicity. American Conference on Pharmacometrics (ACoP6), October 3-9, **2015** Arlington, Virginia - USA.
5. Sobor I, Schlueter S, Othman A, et al. Slowly recovered CYP2E1 after CCl_4 intoxication is associated with less necrosis and more fibrosis. In Environmental Toxicology (ENTOX) in North Rhine-Westphalia, Germany – Interdisciplinary research activities in toxicology, statistic, hygiene and medicine. Scientific symposium, May 7-8, **2015**. Abstracts (p 43), Dortmund-Germany.
6. Othman A, et al.: Three-dimensional reconstruction and quantification of key features of liver microarchitecture. The 31th GASL, January 30-31, **2015**, Munic-Germany.
7. Hammad S, Friebel A, Begher-Tibbe B, Othman A, et al. Role of binucleated hepatocytes in hepatotoxicity and liver regeneration. 80. Jahrestagung der Deutschen Gesellschaft für Experimentelle und Klinische Pharmakologie und Toxikologie e. V. (DGPT) 31. März – 03. April **2014**, Hannover-Germany.
8. Hammad S, von Recklinghausen I, Begher-Tibbe B, Othman A, et al. Reconstruction of the Bile Canaliculicular network: Organization of the healthy adult liver. 1st Virtual Liver Colloquium, **2012**, March 7-8, Dortmund - Germany.
9. Hammad S, Othman A, et al. 5th Milestone Meeting "Cell Therapeutic Approaches in Models of Biliary Fibrosis". March 28, **2011**, Kiel – Germany.
10. Ehnert S, Eipel C, Abshagen K, Othman A, et al. Hepatic differentiation of adipose-derived mesenchymal stem cells reduces recruitment of immune cells after transplantation into livers of CCl_4 treated mice. The 27th congress of German Association for the Studying of the Liver (GASL), January 28-29, **2011**, Regensburg-Germany.
11. Hammad S, Othman A, et al.: 4th Milestone Meeting "Cell Therapeutic Approaches in Models of Biliary Fibrosis". November 09, **2010**, Dortmund – Germany

ACKNOWLEDGEMENTS

First of all I am greatly indebted in my work to our merciful GOD.

I would like to express my cardial gratitude and appreciation to Prof. Dr. Salah Amasheh for his guidance and helpful suggestions. Thanks for the critical observations and corrections. Thank you for giving me always a plenty of time during my talks in Berlin.

I would like also to give tons of thanks to Prof. Dr. Steven Dooley for his professional guidance and supervision throughout my work.

For motivating and collaborations, helpful support and guidance during my work I would like to express my deep thankful to Dr. Roland Hergenröder, my group leader for giving me the chance to continue my work in ISAS Dortmund. He provided me the place and instruments to finish me thesis. Thank you very much for your support, I am appreciating your encourage.

I owe a huge debt of gratitude and appreciation to my co-supervisors in ISAS (Dortmund), Dr. Ahmad Telfah and Dr. Jörg Lambert, neither the words nor the books will express my deep thanks for both of you for helping and supporting me through thick and thin.

Special cardial thank to my co-supervisor Dr. Ahmad Telfah for giving me the chance to work and join his DAAD project. Also travelling to Jordan to attend the Alexander-Von-Humboldt conference is highly appreciated. Thank you very much for your support.

Thousands of tons of thanks to Dr. Jörg Lambert for his help and his critical corrections during the writing time of my thesis.

It was indeed a great opportunity and pleasure working in Grenzflächenprozesse at ISAS-Dortmund. Your collaboration with Medical Faculty Mannheim (Heidelberg University) was a great chance to finalize my work.

ACKNOWLEDGEMENTS

I would like to thank Prof. Dr. Jan G. Hengstler (IfADo-Dortmund) and Dr. med. vet. Seddik Hammad (Medical Faculty Mannheim, Heidelberg University) for the collaborations and guidance.

I would like to thank my colleagues Dr. Christoph Meyer, and Zeribe Nwosu at Medical Faculty Mannheim (Heidelberg University) for their valuable collaborations and support. Special thanks to Prof. Dr. Gianluigi Giannelli (Bari-Italy) who kindly provided the Ly21572599 inhibitor and Julia Werle for MDR2 KO experiment.

I must acknowledge the official assistances and suggestions received from Vassiliki Spiropulu (Institut für Veterinär-Physiologie, Berlin). I would like to acknowledge my thanks to Silke Hankinson (IfADo).

Many thanks to my colleagues at ISAS-Dortmund.

I would like to thank my sisters and my brother for their love and unending support, thank you Marwa, Amira and my brother Ahmad.

For My parents who passed away in 2013 this work is dedicated to both of you.

Finally, I would like to thank my daughters Hanen and Tasneem who helped me during the horrible time and giving me more time for work and writing. I could not have done this work without both of you.

DECLARATION

I, Amnah Hofney Othman, do hereby declare that the research presented in this dissertation was conceived and executed by myself and, apart from the normal guidance from my supervisors, I have received no assistances.

This dissertation is presented in fulfilment of the requirements for the degree Doctor of Veterinary Medicine (DVM).

I hereby grant the University of Berlin free license to reproduce this dissertation, in part or as a whole, for the purpose of research or continuing education.

Amnah Hofney Othman

Date: 17.05.2018

mbvberlin mensch und buch verlag

49,90 Euro | ISBN: 978-3-86387-912-9